

# Inflationary Gravitational Wave Spectral Shapes as test for Low-Scale Leptogenesis

Zafri A Borboruah,<sup>1,\*</sup> Anish Ghoshal,<sup>2,†</sup> Lekhika Malhotra,<sup>1,‡</sup> and Urjit Yajnik<sup>3,1,§</sup>

<sup>1</sup>*Indian Institute of Technology Bombay,  
Mumbai 400076, Maharashtra, India*

<sup>2</sup>*Institute of Theoretical Physics, Faculty of Physics,  
University of Warsaw, ul. Pasteura 5, 02-093 Warsaw, Poland*

<sup>3</sup>*Indian Institute of Technology Gandhinagar, Gandhinagar 382055, India*

## Abstract

We study thermal and non-thermal resonant leptogenesis in a general setting where a heavy scalar  $\phi$  decays to right-handed neutrinos (RHNs) whose further out-of-equilibrium decay generates the required lepton asymmetry. Domination of the energy budget of the Universe by the  $\phi$  or the RHNs alters the evolution history of the primordial gravitational waves (PGW), of inflationary origin, which re-enter the horizon after inflation, modifying the spectral shape. The decays of  $\phi$  and RHNs release entropy into the early Universe while nearly degenerate RHNs facilitate low and intermediate scale leptogenesis. We show that depending on the coupling  $y_R$  of  $\phi$  to radiation species, RHNs can achieve thermal abundance before decaying, which gives rise to thermal leptogenesis. A characteristic damping of the GW spectrum resulting in two knee-like features or one knee-like feature would provide evidence for low-scale thermal and non-thermal leptogenesis respectively. We explore the parameter space for the lightest right-handed neutrino mass  $M_1 \in [10^2, 10^{14}]$  GeV and washout parameter  $K$  that depends on the light-heavy neutrino Yukawa couplings  $\lambda$ , in the weak ( $K < 1$ ) and strong ( $K > 1$ ) washout regimes. The resulting novel features compatible with observed baryon asymmetry are detectable by future experiments like LISA and ET. By estimating signal-to-noise ratio (SNR) for upcoming GW experiments, we investigate the effect of the scalar mass  $M_\phi$  and reheating temperature  $T_\phi$ , which depends on the  $\phi - N$  Yukawa couplings  $y_N$ .

---

\*Electronic address: zafri123@iitb.ac.in

†Electronic address: anish.ghoshal@fuw.edu.pl

‡Electronic address: lekhika.malhotra@iitb.ac.in

§Electronic address: yajnik@iitb.ac.in

## Contents

<b>I. Introduction</b>	3
<b>II. Thermal Leptogenesis</b>	6
A. Conditions for Departure from Thermal Equilibrium	7
B. CP Asymmetry	9
C. Lower Bounds on Heavy Neutrino Masses	9
D. Resonant Leptogenesis	10
<b>III. Non-thermal Leptogenesis via scalar decay</b>	11
A. Set Up	12
B. The Boltzmann Equations	15
<b>IV. Classification of Scenarios</b>	17
A. Analytical Estimates of Equilibrium Temperature	18
B. Dilution Factor from Entropy Injection	19
<b>V. Gravitational Waves of Inflationary Origin</b>	23
A. Primordial spectrum in standard and non-standard cosmology	23
B. Two-step entropy injection	26
C. Signal-to-noise ratio (SNR)	28
D. Bounds from BBN and CMB on dark radiation	30
<b>VI. Results</b>	31
A. Example spectra for different cases	31
B. Estimates for Signal to Noise Ratio	33
C. Compatibility with NANOGrav	36
<b>VII. Discussion &amp; Conclusion</b>	37
<b>Acknowledgments</b>	39
<b>A. Change of Variable</b>	40
<b>B. Thermalization of RHNs</b>	41

## I. INTRODUCTION

The Standard Model (SM) of particle physics is unable to explain tiny neutrino masses and the observed matter-antimatter asymmetry of the Universe. Neutrino oscillation experiments involving solar [1–6], atmospheric [7, 8] and reactor [9–12] neutrinos provide evidence that neutrinos have mass and the flavor states mix due to the propagation of multiple mass eigenstates. This however only quantifies the squared mass differences of the neutrinos and not the absolute mass scales involved. On the other hand, the  $\beta$ -decay experiment KATRIN [13] gives a stringent direct limit on the absolute value of neutrino mass scale,  $m_\nu < 0.8$  eV.

On the cosmological frontiers, measurements of the Cosmic Microwave Background radiation (CMBR) by Planck 2018 [14] and large-scale structure (LSS) constrain the sum of all neutrino masses to  $\sum_i m_{\nu_i} < 0.12$  eV [15, 16]. On the other hand, the observed baryon asymmetry of the Universe (BAU) [15, 17], often expressed in terms of the baryon to photon ratio is, according to the Planck data [15],

$$\eta_B^{\text{CMB}} = \frac{n_B - n_{\bar{B}}}{n_\gamma} = (6.21 \pm 0.16) \times 10^{-10} \quad (1)$$

which is in agreement with the values of abundances of light elements extracted from BBN (Big Bang Nucleosynthesis) data [18].

Just augmenting the Standard Model (SM) with two or more right-handed Majorana neutrinos (RHNs), one can explain the tiny neutrino masses, generated via the well-known Type-I seesaw mechanism [19–22], while baryon asymmetry can be explained using the baryogenesis via leptogenesis mechanism [23], everything tied together under one umbrella. However for this mechanism of baryogenesis to be successful, the lightest RHN mass is required to exceed the Davidson-Ibarra bound,  $M_1 \gtrsim 10^9$  GeV, assuming the RHN mass spectrum is hierarchical, and also assuming no lepton flavor effects [24–28]. This destroys any hope of direct detection of the high-scale seesaw and leptogenesis as they lie well beyond the energy reach of the current or foreseeable future laboratory experiments or astrophysical observations making it impossible to test such new physics.

Nonetheless, certain indirect signatures of new physics like lepton number violation processes through neutrinoless double beta decay [29] or CP violation in neutrino oscillation [30]

are searched for in laboratories. On the other hand, theoretical constraints on the low energy values of couplings, consistent with UV-completion such as  $SO(10)$  Grand Unified Theories (GUT) [31–37] or with the requirement of electroweak (EW) vacuum (meta)stability in the early Universe [38, 39] allow us to pose some bounds on the large parameter space involved in seesaw and leptogenesis.

The discovery of Gravitational Waves (GWs) from black hole mergers by LIGO and Virgo collaboration [40, 41] and evidence for measurements of stochastic GW background by pulsar timing array (PTA) observations [42–48] have lead to several new physics cases to detect GWs of primordial origins as well. Particularly in the context of baryogenesis via leptogenesis, cosmological pathways to probe such high-scale physics involve predictions of the CMB spectral indices [49] or gravitational waves from local cosmic strings [50–53], global cosmic strings [54], domain walls [55, 56], nucleating and colliding vacuum bubbles [57, 58], other topological defects [59], graviton bremsstrahlung [60], inflationary tensor perturbations propagating as GW [61, 62], primordial blackholes [63–70], and exploring the oscillatory features of the primordial non-gaussianity and curvature bi-spectrum and tri-spectrum [71, 72].

Under this circumstance, we need more such probes of BSM physics and form a synergy between cosmological observations and laboratory experiments involving seesaw and low-scale leptogenesis. In this paper, we take a first step in this direction and investigate a general scenario where a heavy scalar denoted by  $\phi$  may decay to create an initial non-thermal abundance of right-handed neutrinos (RHN) whose subsequent decays lead to leptogenesis satisfying Eq. (1). We will be concerned with Gravitational Waves that are generated due to quantum tensor fluctuations of the metric during inflation [73–76]. These GWs can act as a book-keeping of the expansion history of our Universe [77–85]. Since the detailed time evolution of the Hubble rate during the expansion determines various PGW frequencies that are red-shifted to the present day, thus allowing us to investigate standard and non-standard thermal history of the universe in the pre-BBN era [85–95]. In this context, since we are interested in low scale seesaw and leptogenesis, we will study a scenario where  $\phi$  dominates the energy budget of the Universe which leads to interesting GW spectral shapes. On one hand,  $\phi$  decay will facilitate low-scale leptogenesis and on the other hand, it is also responsible for the generation of GW spectral shapes that can be measured by various GW detectors. In particular, we consider an epoch of intermediate matter domination by  $\phi$

particles affecting the post-inflationary evolution of the Universe [96–98].

We will study GW probes of both thermal and non-thermal low scale leptogenesis scenarios. The leptogenesis scale is brought down mainly by the resonance effect that enhances the CP parameter  $\epsilon$ . Non-thermal leptogenesis is achieved via the scalar decay to RHNs. Non-thermal production of RHN creates an excess initial abundance of RHNs after the scalar has decayed, compared to the thermal case. Depending on reheating temperature  $T_\phi$  and washout parameter  $K$ , the final efficiency factor  $\kappa_f$  may get enhanced compared to the thermal case due to this excess initial abundance [99, 100]. Unlike [61], here the RHNs need not dominate the Universe since the scalar is assumed to dominate the energy density of the Universe which distorts inflationary GWs. Therefore we do not need to stick to only the  $K \ll 1$  condition of [61] for RHN domination. Note that RHNs can still dominate after  $\phi$  decays, depending on parameters.

The decays occur very far away from thermal equilibrium, therefore it is bound to release a large amount of entropy dump, which in turn dilutes the energy density of primordial GWs that enter the horizon before the decay. We show that if the scalar couples directly to the radiation bath, under appropriate conditions RHNs produced non-thermally from  $\phi$  thermalize quickly with the radiation bath, in which case entropy is injected in two stages, one from scalar decay and the other from RHN decay if they dominate the energy budget of the Universe before decaying. In this case, two knee-like features occur in the GW spectrum due to the scalar decay which we show for the first time. We will show the capability of several upcoming GW detectors like LISA, DECIGO, BBO, etc. in probing the parameter space for such leptogenesis, particularly in regions where it is impossible to test via laboratory or astrophysical experiments.

*The paper is organized as follows:* In Sec. II, we give a brief overview of the thermal leptogenesis mechanism and the Davidson-Ibarra bound on heavy neutrino masses. We consider resonant leptogenesis to bring the leptogenesis scale down. In Sec. III, we discuss the non-thermal leptogenesis scenario from scalar decay and the relevant Boltzmann equations. In Sec. IV, we identify three classes of scenarios relevant to GW observations, two of which correspond to non-thermal and one to thermal leptogenesis. We provide analytical approximations of matter-radiation equilibrium temperature and dilution factor from entropy injection for these classifications. Then in Sec. V we discuss primordial gravitational waves from inflation with and without an intermediate matter domination epoch. We

also introduce a transfer function to encapsulate a 2-step entropy injection. This section is followed by our results in Sec. VI. Finally, we conclude this paper in Sec. VII.

## II. THERMAL LEPTOGENESIS

Before discussing the effect of scalar field reheating on leptogenesis let us first we give a brief review of standard thermal leptogenesis in this section. Initially proposed by Fukugita and Yanagida in 1986 [23, 101], thermal leptogenesis hinges on the out-of-equilibrium decay of RHNs, which are thermally produced through scattering processes in the early Universe from the thermal bath of the primordial SM plasma. The Lagrangian is given by,

$$\mathcal{L}_{\text{thermal}} = \mathcal{L}_{\text{SM}} + i\bar{N}\not{\partial}N - \left( \lambda\bar{L}\tilde{H}N + \frac{M_N}{2}\overline{N^c}N + \text{h.c.} \right) \quad (2)$$

where  $\mathcal{L}_{\text{SM}}$  is the SM Lagrangian,  $N$  represents RHNs,  $\tilde{H} = i\sigma_2 H^*$  where  $H$  is the SM Higgs doublet and  $L$  is the SM leptonic doublet. Here  $M_N = \text{diag}[M_1, M_2, M_3]$  is the RHN Majorana mass matrix and  $\lambda$  encompasses the light-heavy Yukawa couplings. Due to the Majorana mass term of RHNs, after electroweak symmetry breaking (EWSB), the familiar Type-I seesaw mechanism [20] provides mass to the light neutrinos,  $m_\nu = v^2\lambda M_N^{-1}\lambda^T$ , where  $v \sim 174$  GeV is the vacuum expectation value (VEV) of the SM Higgs. On the other hand, RHNs of Majorana nature, can decay into both leptons and anti-leptons through the Yukawa coupling matrix  $\lambda$ , thereby violating lepton number (LNV),

$$N_1 \rightarrow H + L \quad \text{and} \quad N_1 \rightarrow H^\dagger + L^\dagger \quad (3)$$

Typically, this scenario assumes a hierarchical heavy neutrino mass spectrum, where the masses of the heavier RH neutrinos,  $M_2$  and  $M_3$ , are much greater than the lightest RHN mass,  $M_1$ . This condition allows the lightest neutrino,  $N_1$  to generate the necessary lepton asymmetry when CP is violated in their decay, after washing out any asymmetry created by  $N_2$  and  $N_3$ . The CP asymmetry, denoted as  $\epsilon_1$ , is given by:

$$\epsilon_1 = \frac{\Gamma_{N_1 \rightarrow HL} - \Gamma_{N_1 \rightarrow H^\dagger L^\dagger}}{\Gamma_{N_1}^{rf}} \quad (4)$$

where  $\Gamma_{N_1 \rightarrow Hl}$  is the decay width of the  $N_1 \rightarrow H + l$  decay and

$$\Gamma_{N_1}^{rf} = \Gamma_{N_1 \rightarrow HL} + \Gamma_{N_1 \rightarrow H^\dagger L^\dagger} = \frac{|\lambda\lambda^\dagger|_{11}}{8\pi} M_1 \quad (5)$$

is the total decay width of  $N_1$  in the rest frame of the neutrino. The lepton asymmetry can be re-written as  $B - L$  asymmetry denoted by the number density  $n_{B-L}$ , which is subsequently converted into the baryon asymmetry through  $B + L$  conserving electroweak sphaleron processes [102–104]. When there is no initial  $B - L$  asymmetry, the final baryon asymmetry, denoted as baryon-to-photon number density ratio  $\eta_B$ , is expressed as [105],

$$\eta_B \equiv \frac{n_B - n_{\bar{B}}}{n_\gamma} = -\frac{3}{4} \frac{a_{\text{sph}}}{f} \epsilon_1 \kappa_f \equiv -d \epsilon_1 \kappa_f \simeq 0.96 \times 10^{-2} \epsilon_1 \kappa_f \quad (6)$$

where  $a_{\text{sph}} = 28/79$  [102, 103, 106] is the efficiency of the sphaleron processes of converting  $B - L$  asymmetry into baryon asymmetry and  $f = 2387/86$  is the dilution factor due to production of photons since the onset of leptogenesis till recombination assuming an isentropic expansion of the Universe. And  $\kappa_f$  is the *efficiency parameter* [105], which is independent of  $\epsilon_1$  and which parameterizes the efficiency of lepton asymmetry production depending on the initial  $N_1$  abundance and washout. It can be calculated by solving the relevant Boltzmann equations governing the evolution of the  $N_1$  abundance and  $B - L$  asymmetry [107, 108]. Its final value is normalized to unity if thermal initial abundance of  $N_1$  is assumed and there is no washout.

### A. Conditions for Departure from Thermal Equilibrium

One of the key conditions for successful baryogenesis, as outlined by Sakharov, is the departure from thermal equilibrium. In the context of leptogenesis, this condition is satisfied if the total decay rate of  $N_1$  is smaller than the Hubble expansion rate of the Universe when the temperature is approximately equal to the mass of  $N_1$ :

$$\Gamma_{N_1}^{r,f} < \mathcal{H}(T \sim M_1) \quad (7)$$

where  $\mathcal{H}(T \sim M_i) \equiv \mathcal{H}(M_i) = \sqrt{\frac{8\pi^3 g_*}{90} \frac{M_i^2}{M_{\text{pl}}}}$  is the Hubble parameter with  $M_{\text{pl}} = 1.22 \times 10^{19}$  GeV and  $g_*$  is the relativistic degrees of freedom which is approximately equal to 106.75 at the high temperatures under discussion. It can be shown that the above condition is satisfied when the *effective neutrino mass*, defined by,

$$\tilde{m}_1 = \frac{(m_D^\dagger m_D)_{11}}{M_1} \quad (8)$$

where  $m_D = \lambda v$  is the Dirac mass matrix with  $v = \langle H \rangle \simeq 174$  GeV being the vacuum expectation value (VEV) of the Standard Model Higgs, is smaller than the *equilibrium*

neutrino mass, defined as,

$$m_* = \frac{16\pi^{5/2}}{3\sqrt{5}} g_*^{1/2} \frac{v^2}{M_{\text{pl}}} \simeq 1.1 \times 10^{-3} \text{ eV} \quad (9)$$

The ratio is called the decay parameter,

$$K \equiv \frac{\Gamma_{N_1}^{rf}}{\mathcal{H}(M_1)} = \frac{\tilde{m}_1}{m_*} \quad (10)$$

which determines whether  $N_1$  decays are in thermal equilibrium or not. The case  $K < 1$  is called the *weak washout regime*, where Yukawa interactions of  $N_1$  with light neutrinos via the SM Higgs are weak, hence washout of any initial asymmetry via reverse processes is small. Therefore leptogenesis is unavoidable in this regime. However in the so called *strong washout regime* ( $K > 1$ ), although Yukawa interactions are strong, leptogenesis can still occur and the final asymmetry depends on the interplay between decay, inverse decay and scattering of RHNs [105].

It turns out the final efficiency parameter  $\kappa_f$  can be estimated analytically for both weak and strong washout regime [105]. In the strong washout regime,  $\kappa_f$  is estimated by,

$$\kappa_f(K) \simeq (2 \pm 1) \times 10^{-2} \left( \frac{0.01 \text{ eV}}{m_* K} \right)^{1.1 \pm 0.1} \quad (11)$$

while in the weak washout regime,  $\kappa_f$  depends on the initial abundance of  $N_1$ . For thermal initial abundance, it is approximately 1 in the weak regime while for vanishing initial abundance, it is estimated as,

$$\kappa_f(K) \simeq \frac{9\pi^2 K^2}{64}, \quad (K < 1) \quad (12)$$

For thermal initial  $N_1$  abundance,  $\kappa_f$  can be generically written for all  $K$  as,

$$\kappa_f(K) \simeq \frac{2}{z_B(K)K} \left( 1 - e^{\frac{1}{2}z_B(K)K} \right) \quad (13)$$

$$\text{where } z_B(K) \simeq 1 + \frac{1}{2} \ln \left( 1 + \frac{\pi K^2}{1024} \left[ \ln \left( \frac{3125\pi K^2}{1024} \right) \right]^5 \right) \quad (14)$$

In Fig. 2 we show  $\kappa_f$  as a function of washout parameter  $K$  for thermal (red solid line) and vanishing (blue dashed line) initial abundance of  $N_1$ . Depending on the CP parameter  $\epsilon_1$  and  $K$ , the final baryon asymmetry can be calculated from Eq. (6).

## B. CP Asymmetry

The CP asymmetry  $\epsilon_1$  is determined by the interference between the tree level and 1-loop diagrams [109, 110] and can be calculated from  $lH \rightarrow lH$  scattering processes [111]. The relevant Feynmann diagrams giving tree level, vertex and self-energy contributions are shown in Fig. 1.

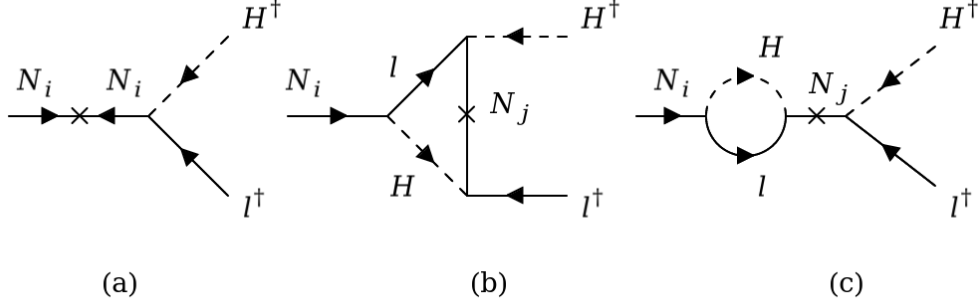


FIG. 1: *Feynmann diagrams of  $N \rightarrow lH$  decay process at the (a) tree-level and (b)-(c) 1-loop level. (b) represents the vertex contribution and (c) represents self-energy contribution.*

The maximal asymmetry is obtained for  $M_{2,3} \gg M_1$  and light neutrino masses  $m_1 \sim \tilde{m}_1$ ,  $m_3 = \sqrt{m_{\text{atm}}^2 + m_1^2}$  [27, 99, 112–114],

$$\epsilon_1^{\text{max}} = \frac{3}{16\pi} \frac{M_1}{v^2} (m_3 - m_1) \simeq 10^{-6} \left( \frac{M_1}{10^{10} \text{ GeV}} \right) \left( \frac{m_3 - m_1}{0.05 \text{ eV}} \right) \quad (15)$$

## C. Lower Bounds on Heavy Neutrino Masses

Putting the maximal CP asymmetry parameter  $\epsilon_1^{\text{max}}$  in Eq. (6) gives the maximal baryon asymmetry  $\eta_B^{\text{max}}$ , which needs to be larger than the observed asymmetry  $\eta_B^{\text{CMB}}$ , i.e.  $\eta_B^{\text{max}} \geq \eta_B^{\text{CMB}}$ . Then one finds the Davidson-Ibarra bound on  $M_1$  using Eq. (6) [27, 105, 115],

$$M_1 \geq 6.4 \times 10^8 \text{ GeV} \left( \frac{\eta_B^{\text{CMB}}}{6 \times 10^{-10}} \right) \left( \frac{0.05 \text{ eV}}{m_3 - m_1} \right) \kappa_f^{-1} \quad (16)$$

Assuming the final efficiency factor  $\kappa_f = 1$  gives the  $3\sigma$  bound on the minimum reheating temperature  $T_{\text{RH}}$  at the end of inflation [113],

$$T_{\text{RH}} \gtrsim M_1 \gtrsim 4 \times 10^8 \text{ GeV} \quad (17)$$

This stems from the condition that  $T_{\text{RH}}$  needs to be larger than the initial temperature of leptogenesis  $T_i \sim M_1$  when the RHN decay process becomes out-of-equilibrium (see Eq. (7)) [116].

#### D. Resonant Leptogenesis

Thermal leptogenesis operates at high temperatures, which in turn pushes the inflationary reheating temperature  $T_{\text{RH}}$  to a high scale, as shown in Eq. (16) and (17). Such high scales involving RHN masses  $M_i \gtrsim 10^9$  GeV are difficult to test in the lab. Also a high neutrino mass is in conflict with Electroweak naturalness condition which requires RHN masses  $M_i \lesssim 10^7$  GeV [117–119]. A lower reheating temperature from inflation  $T_{\text{RH}}$  is motivated in different inflationary scenarios like [120, 121]. Even in some SUGRA models [122], reheating temperature is found to be as low as  $10^6$  GeV which contradicts a high  $T_{\text{RH}}$ , favouring low-scale-leptogenesis. Motivated by these reasons, and for lab testability, the scale of leptogenesis can be brought down by several orders in the so called *resonant* regime which focuses on nearly degenerate heavy neutrinos leading to pronounced CP violation in their decays. It can be shown that if the mass difference between the two lightest right-handed neutrinos is of the order of the decay widths of them, i.e.  $M_2 - M_1 \sim \Gamma_{N_2}^{rf}$  the CP parameter  $\epsilon_1$  is enhanced via the self-energy contribution [114, 123] in the loop level diagrams shown in Fig 1.

The maximum CP asymmetry with resonant effect due to quasi-degenerate right-handed neutrinos  $N_1$  and  $N_2$  can be written as [61, 114],

$$\epsilon = \text{Min} \left[ \epsilon_1^{\text{max}} \frac{S_2 \cdot m_3 - m_1}{m_3 - m_1}, 1 \right], \quad \text{where } S_2 = \frac{M_2}{2\Gamma_{N_2}^{rf}} \quad \text{and } M_2 - M_1 = \frac{\Gamma_{N_2}^{rf}}{2} \quad (18)$$

where,  $\epsilon_1^{\text{max}}$  is the maximal asymmetry in non-resonant case given by Eq. (15). It was shown that within the resonant regime the lowest RHN mass  $M_1$  can be as low as 1 TeV [124]. In [125] this scale is shown to reach upto the electroweak symmetry breaking scale  $\sim 100$  GeV, below which sphaleron processes are suppressed and the lepton asymmetry can not be effectively converted to baryon asymmetry. From here onwards we will consider resonant leptogenesis with  $M_1 \gtrsim 100$  GeV for our analysis. Note that in some alternate leptogenesis scenarios, e.g. via neutrino oscillations, BAU can be generated for even for RHN mass values  $\sim 100$  MeV [126].

### III. NON-THERMAL LEPTOGENESIS VIA SCALAR DECAY

In vanilla leptogenesis, RHNs are in thermal equilibrium at production. However, it is possible to produce RHNs non-thermally from inflaton [28, 99, 100, 127] or a generic scalar decay [119, 128]. Such a scenario can lead to excess initial abundance of RHNs compared to their thermal abundance. As a result the final efficiency factor,  $\kappa_f$  can be enhanced upto  $\mathcal{O}(2)$  which relaxes the Davidson-Ibarra bound on RHN mass given in Eq. 16. Note that the RHNs can also be produced thermally from the scalar which is similar to thermal leptogenesis. We consider the Lagrangian [49],

$$\mathcal{L}_{\text{nonthermal}} = \mathcal{L}_{\text{thermal}} - \left( \frac{y_N}{2} \phi \overline{N^C} N + \frac{y_R}{2} \phi \bar{f} f + \text{h.c.} \right) \quad (19)$$

where  $f$  represents a Dirac fermion which is in thermal equilibrium with the radiation bath. This kind of Lagrangian can be obtained by considering for example a gauged  $U(1)$  extension [49, 129] of the SM where the vector-like fermions  $f$  can couple to the SM sector via the  $U(1)$  gauge boson. We will assume the scalar mass to always exceed twice the right-handed neutrino masses,  $M_\phi > 2M_1$  where  $M_1$  is the mass of the lightest RH neutrino. The decay width of  $\phi$  to RH neutrinos is [39, 49],

$$\Gamma_{\phi \rightarrow N_i N_i} \simeq \frac{y_{N_i}^2 M_\phi}{16\pi} \sqrt{1 - \frac{4M_i^2}{M_\phi^2}} \quad (20)$$

where  $i = 1, 2, 3$  represents the 3 RH neutrinos. On the other hand, decay width of the scalar to radiation is given by [49, 130],

$$\Gamma_{\phi \rightarrow R} \simeq \frac{y_R^2 M_\phi}{8\pi} \quad (21)$$

where subscript  $\phi \rightarrow R$  denotes  $\phi$  decaying to radiation via the Dirac fermions  $f$  in Eq. (19) which are in thermal equilibrium with the SM bath. We define the branching ratios,

$$\text{BR}(\phi \rightarrow N_i N_i) \equiv \frac{\Gamma_{\phi \rightarrow N_i N_i}}{\Gamma_\phi}, \quad \text{BR}(\phi \rightarrow R) \equiv \frac{\Gamma_{\phi \rightarrow R}}{\Gamma_\phi} \quad (22)$$

where  $\Gamma_\phi = \sum_i \Gamma_{\phi \rightarrow N_i N_i} + \Gamma_{\phi \rightarrow R}$  is the total decay width of  $\phi$ . Essentially,  $\text{BR}(\phi \rightarrow N_i N_i)$  is dependent on the coupling  $y_R$ , so decreasing  $y_R$  will increase  $\text{BR}(\phi \rightarrow N_i N_i)$ . If  $y_R \sim 0$  then  $\text{BR}(\phi \rightarrow N_i N_i) \sim 1$  which leads to maximum non-thermal RHN production from  $\phi$  hence maximum lepton asymmetry.

We assume a resonant leptogenesis scenario with  $M_1 \sim M_2 \ll M_3$  such that the scalar dominantly decays to the two lightest RHNs,  $N_1$  and  $N_2$ . The resonance effect makes sure that enough asymmetry is generated for all  $M_1$  values starting from 100 GeV, to explain the BAU. RHNs can be in thermal equilibrium with the radiation bath either via their Yukawa couplings  $\lambda$  or via the 2-to-2 scattering process  $N_i N_i \leftrightarrow \bar{f} f$  via  $\phi$  for non-vanishing values of  $y_R$ . See appendix B for more details. During this paper, we take  $y_R = 0$  when discussing non-thermal leptogenesis and only consider non-zero  $y_R$  when demonstrating thermal leptogenesis. We treat the independent variables for our analysis to be  $M_i$ ,  $M_\phi$ ,  $\lambda$  and  $y_{N_i}$ . Later in Sec. III we will parameterize  $\lambda$  and  $y_{N_i}$  in terms of the decay temperatures of the scalar  $T_\phi$  and right-handed neutrinos  $T_{N_i}$ .

We consider the parameter space of the scalar where it dominates the energy budget of the Universe before decaying, leading to a phase of matter dominated pre-BBN era. The RHNs produced from scalar decay, as we shall see, may or may not further dominate the energy density depending on the parameters used. Their out-of-equilibrium decay to relativistic SM particles will inject considerable amount of entropy into the Universe. This dampens the primordial gravitational waves from inflation that re-enters the horizon during the early matter domination epoch. We show such signature of low-scale leptogenesis in primordial gravitational waves can be detected in various GW experiments such as BBO, DECIGO,  $\mu$ -ARES, ET, LISA, CE etc.

### A. Set Up

We consider the scalar  $\phi$  was in thermal equilibrium with the primordial plasma after the end of inflation either via its direct coupling with SM particles, or via indirect interactions, e.g. coupling with inflaton field in a specific inflationary model or vector-like fermions in a gauged  $U(1)$  extension of the SM mentioned above. Then the scalar froze out at some temperature  $T_f$  and eventually it dominates the energy budget of the Universe at temperature  $T_{\text{dom}}$ . If the freeze out happens while the scalar particles were still relativistic we obtain the maximal  $\phi$  abundance [97, 98],

$$\frac{n_\phi}{s} \Big|_f = \frac{45 \zeta(3)}{2\pi^4 g_{*S}} \quad (23)$$

where subscript  $f$  denotes the time of freeze-out,  $n_\phi$  is the number density of  $\phi$  and the entropy density is given by,

$$s = \frac{2\pi^2}{45} g_{*S} T^3 \quad (24)$$

The effective degrees of freedom related to entropy is denoted by  $g_{*S}$  which we take to be equal to  $g_* = 106.75$  at high temperatures for simplicity in our analysis. After freeze-out,  $\phi$  eventually becomes non-relativistic after which its energy density red-shifts as matter and dominates over the radiation density starting from temperature [97, 131],

$$T_{\text{dom}} \sim \frac{M_\phi}{g_*} \approx 0.01 M_\phi \quad (25)$$

The  $\phi$ -dominated phase starts at temperature  $T_{\text{dom}}$  and ends at some temperature decay temperature  $T_\phi$ ; we always assume  $T_\phi < T_{\text{dom}}$  such that we get a period of time in early Universe of scalar era. The dynamics of  $\phi$  and its decay products into RHNs and radiation can be obtained by solving the relevant Boltzmann equations which we will describe in Sec. III B.

We start with Eq. (20) and (21), the partial decay widths of  $\phi$  to lightest RHNs and radiation and consider only the two lightest RHNs  $N_1, N_2$ . The branching ratios are given by (22). As long as mass of the scalar  $M_\phi > 2M_{1,2}$ , the scalar can decay to  $N_1$  and  $N_2$ .

The RHNs  $N_1, N_2$  further decay to lepton-Higgs pairs with the thermally averaged decay widths,

$$\Gamma_{N_i} = \Gamma_{N_i}^{rf} \frac{K_1(z)}{K_2(z)} \sim \mathcal{H}(M_i) K \frac{K_1(z)}{K_2(z)}, \quad (26)$$

where  $\mathcal{H}(M_i) = \sqrt{\frac{8\pi^3 g_*}{90} \frac{M_i^2}{M_{\text{pl}}}}$  is the Hubble parameter with  $M_{\text{pl}} = 1.22 \times 10^{19}$  GeV.  $K_1(z), K_2(z)$  are the modified Bessel functions of first and second kind and  $z = M_i/T$ .

The decay temperatures of the scalar or the RHNs are calculated assuming that the energy density of scalar/RHN is converted instantaneously into radiation [99],

$$T_\phi = \left( \frac{90}{8\pi^3 g_*(T_\phi)} \right)^{\frac{1}{4}} \sqrt{\Gamma_\phi M_{\text{pl}}} \quad (27)$$

$$T_{N_i} = \left( \frac{90}{8\pi^3 g_*(T_{N_i})} \right)^{\frac{1}{4}} \sqrt{\Gamma_{N_i}^{rf} M_{\text{pl}}} = M_i \sqrt{K} \quad (28)$$

where  $\Gamma_\phi \sim \Gamma_{\phi \rightarrow N_1 N_1} + \Gamma_{\phi \rightarrow N_2 N_2} + \Gamma_{\phi \rightarrow R}$  is the total decay width of  $\phi$  and  $g_*(T)$  is the relativistic degree of freedom at the corresponding temperature  $T$  which is taken to be

$\sim 106.75$ . Using Eq. (20) (21) in Eq. (27) and considering Eq. (25), we can write the condition  $T_\phi < T_{\text{dom}}$  in terms of couplings as,

$$y_{N_i}^2 + y_R^2 \lesssim \frac{M_\phi}{M_{\text{pl}}} \quad (29)$$

where  $i = 1, 2$  and we have considered  $M_1, M_2 \ll M_\phi$ . We can expect that the latest radiation dominated era starts at either  $T_\phi$  or  $T_{N_1}$  depending on which one is lower. Notice that reheating temperature  $T_{\text{RH}}$  after inflation now need not be larger than  $M_1$  as in the thermal case. Rather  $T_{\text{RH}}$  only needs to be roughly larger than  $T_{\text{dom}}$  now, since RHNs are produced dominantly at  $T_\phi < T_{\text{dom}}$  from  $\phi$  decay, regardless of their masses.

In Table I, we summarize all the necessary conversion formulas for the parameters used in our analysis in terms of the couplings and masses of the scalar and RHNs.

Variable	Symbol	Definition
RHN decay width in the rest frame	$\Gamma_{N_i}^{rf}$	$\frac{ \lambda ^2 M_i}{8\pi}$
Scalar decay width to RHNs	$\Gamma_{\phi \rightarrow N_i N_i}$	$\frac{y_{N_i}^2 M_\phi}{16\pi} \sqrt{1 - \frac{4M_i^2}{M_\phi^2}}$
Scalar decay width to radiation	$\Gamma_{\phi \rightarrow R}$	$\frac{y_R^2 M_\phi}{8\pi}$
Total decay width of scalar	$\Gamma_\phi$	$\Gamma_{\phi \rightarrow N_1 N_1} + \Gamma_{\phi \rightarrow N_2 N_2} + \Gamma_{\phi \rightarrow R}$
Scalar decay temperature	$T_\phi$	$\left(\frac{90}{8\pi^3 g_*(T_\phi)}\right)^{\frac{1}{4}} \sqrt{\Gamma_\phi M_{\text{pl}}}$ $\sim 0.05 \sqrt{y_{N_1}^2 + y_R^2} \left(\frac{100}{g_*(T_\phi)}\right)^{\frac{1}{4}} \sqrt{M_\phi M_{\text{pl}}}$
Washout parameter	$K$	$\frac{\tilde{m}_1}{m_*} = \frac{\tilde{m}_1}{1.1 \times 10^{-3} \text{ eV}} = \frac{ \lambda _1^2 v^2 / M_1}{1.1 \times 10^{-3} \text{ eV}}$
RHN decay temperature	$T_{N_1}$	$\left(\frac{90}{8\pi^3 g_*(T_\phi)}\right)^{\frac{1}{4}} \sqrt{\Gamma_{N_1}^{rf} M_{\text{pl}}} \sim M_1 \sqrt{K}$

TABLE I: *Definition of the relevant parameters used for our analysis in terms of couplings and masses of the scalar and RHNs. Here  $v = 174 \text{ GeV}$  is the electroweak VEV,  $\lambda$  is the Yukawa coupling of RHNs with active neutrinos via SM Higgs. Here we also considered resonant scenario,*

$$\text{i.e. } y_{N_1} \sim y_{N_2} \ll y_{N_3}.$$

## B. The Boltzmann Equations

The evolution of the energy densities of matter and radiation and the number density of  $B - L$  asymmetry are determined by the Boltzmann equations,

$$\begin{aligned}
\dot{\rho}_\phi &= -3\mathcal{H}\rho_\phi - \Gamma_\phi \rho_\phi \\
\dot{\rho}_{N_1} &= -3\mathcal{H}\rho_{N_1} + \Gamma_{\phi \rightarrow N_1 N_1} \rho_\phi - \Gamma_{N_1}(\rho_{N_1} - \rho_{N_1}^{eq}) \\
\dot{\rho}_{N_2} &= -3\mathcal{H}\rho_{N_2} + \Gamma_{\phi \rightarrow N_2 N_2} \rho_\phi - \Gamma_{N_2}(\rho_{N_2} - \rho_{N_2}^{eq}) \\
\dot{n}_{B-L} &= -3\mathcal{H}n_{B-L} - \epsilon \sum_{i=1}^2 \Gamma_{N_i}(n_{N_i} - n_{N_i}^{eq}) - \Gamma_{ID} n_{B-L} \\
\dot{\rho}_R &= -4\mathcal{H}\rho_R + \Gamma_{\phi \rightarrow R} \rho_\phi + \sum_{i=1}^2 \Gamma_{N_i}(\rho_{N_i} - \rho_{N_i}^{eq})
\end{aligned} \tag{30}$$

where  $\mathcal{H}$  is the Hubble parameter in cosmic time and dot denotes derivative with respect to cosmic time and  $\rho_X^{eq}$  and  $n_X^{eq}$  represents the equilibrium energy and number density of the species  $X$  respectively.  $\Gamma_{ID}$  is the inverse decay rate. See Appendix A for details. Here we have considered only decays and inverse decays and neglected scattering processes of the RHNs and the scalar. Also, for simplicity here we considered only non-relativistic RHN production in the equations for  $N_{1,2}$ , which may not be guaranteed when  $M_\phi \gg M_{1,2}$ .

While solving the Boltzmann equations we take the coupling  $y_R = 0$  defined in Eq. (19) such that  $\Gamma_{\phi \rightarrow R} \sim 0$  in order to maximize the RHN production from  $\phi$  and hence the lepton asymmetry. Later we will consider the  $y_R > 0$  scenario which is similar to thermal leptogenesis. We start solving the Boltzmann equations from the time when the scalar energy density overtakes the radiation energy density. Thus the initial energy density of the scalar is equal to the radiation density [97],

$$\rho_\phi(T_{\text{dom}}) = \rho_R(T_{\text{dom}}) = \frac{\pi^2}{30} g_*(T_{\text{dom}}) T_{\text{dom}}^4 \tag{31}$$

We take  $T_{\text{dom}}$  from Eq. (25). The initial densities of RHNs are taken to be free parameters smaller than  $\rho_\phi(T_{\text{dom}})$  while initial  $B - L$  asymmetry is taken to be negligible. Further details on the numerical solution of the Boltzmann equations and calculation of final  $\kappa_f$  value as-well-as maximum available temperature are given in Appendix A. In Fig. 2 along with the thermal case we also show the enhancement in  $\kappa_f$  in non-thermal leptogenesis from  $\phi$  decay by solving the Boltzmann equations (30). The solid magenta line, dashed green line and the dash-dotted purple line shows the final efficiency factor as a function of the washout

parameter for a special case,  $M_1 \sim T_\phi$  [99]. Here we took  $M_1 = 10^5$  GeV,  $M_\phi = 10^8$  GeV and  $T_\phi = 10^5, 5 \times 10^4, 10^4$  GeV. Efficiency factor is maximum at  $K \sim 0.3$  for  $M_1 \sim T_\phi$ . We note that for  $T_\phi \ll M_1$ , the final efficiency factor becomes independent of  $K$ .

At this point we are able to numerically calculate the final baryon asymmetry in our model. However we are not interested in the exact amount of asymmetry generated, since our goal is studying GW probe of leptogenesis. In the next section we discuss classification of scenarios based on numerical results and analytical approximations, relevant for GW sensitivity. We make sure that for all cases, observed BAU is successfully generated.

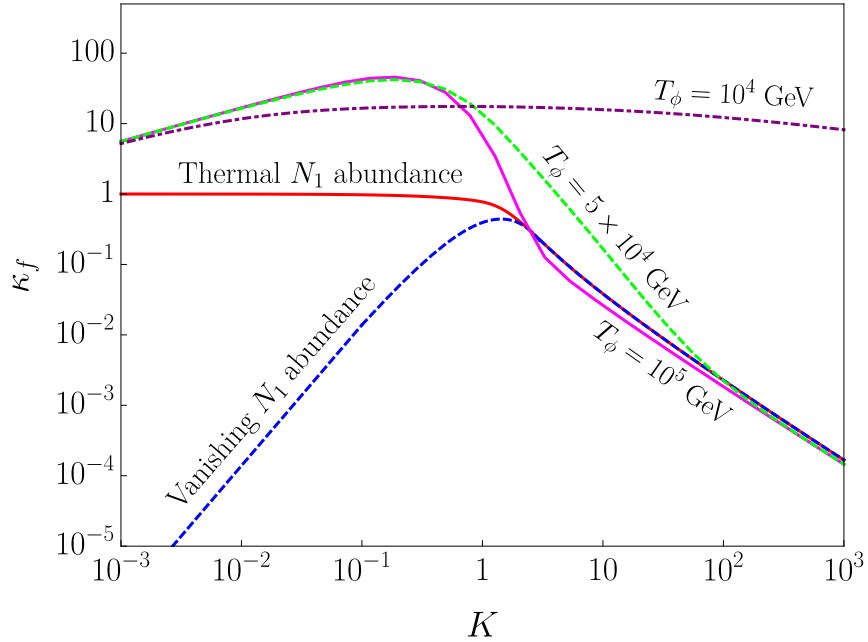


FIG. 2: Analytical estimate of final efficiency factor  $\kappa_f$  as a function of washout parameter  $K$  in thermal and numerical solutions to the Boltzmann equations (30) in non-thermal leptogenesis.

Red solid curve represents thermal initial abundance of  $N_1$  and blue dashed curve represents vanishing initial  $N_1$  abundance in thermal leptogenesis. Here we used Eq. (13) and (14) for the blue curve while for the red curve we use Eq. (12) for  $K \ll 1$  and interpolate it to the thermal case in the  $K \gg 1$  regime. The solid magenta, dashed green and dash-dotted purple lines represent non-thermal leptogenesis with  $M_1 = 10^5$  GeV,  $M_\phi = 10^8$  GeV for different  $T_\phi$  values.

#### IV. CLASSIFICATION OF SCENARIOS

In this section, we identify two general non-thermal scenarios relevant for GW observations along the lines of [100]. Additionally we introduce a thermal leptogenesis scenario with two-step entropy injection. We present analytical estimates of the equilibrium temperature when matter domination ends, and the dilution factor from entropy injection for each of the three scenarios. In all the cases, the resonantly enhanced final asymmetry is higher than the observed asymmetry of the Universe for  $M_1 \gtrsim 100$  GeV as discussed in the previous sections. In brief, the three scenarios are,

1. *Case (a): Instantaneous RHN decay* - Portrayed in Fig. 3, we classify this scenario by requiring  $\Gamma_N \gg \Gamma_\phi$  which implies  $T_{N_1} \gg T_\phi$ . This means that the RHNs are mostly produced at temperatures around  $T_\phi$ , when the scalar completely decays away and radiation starts dominating again. Those RHNs instantaneously decay to the SM bath. Even in the strong washout case  $K \gg 1$ , RHNs do not have time to thermalize with the radiation bath, thus the RHN decay process is strongly out-of-equilibrium. The evolution of the energy densities of different matter and radiation are shown in Fig. 3 for both weak ( $K \ll 1$ ) and strong ( $K \gg 1$ ) washout regime. We can see that for strong washout, the RHN density is lower than the weak washout case due to higher decay rate. From GW perspective, this case is only dependent of the total decay width of  $\phi$  and independent of partial decay widths to RHNs and radiation, i.e. independent of the coupling  $y_R$  given in Eq. (19). However the amount of leptogenesis depends on  $y_R$ .
2. *Case (b): RHN Domination* - For this scenario we need  $y_R \sim 0$ , and  $\Gamma_N \ll \Gamma_\phi$  implying  $T_{N_1} \ll T_\phi$  which means the RHN decay is delayed after production. As shown in Fig. 4, RHNs start to dominate the energy density as soon as the scalar decays away, with no radiation domination in between. When the RHNs decay out-of-equilibrium, radiation domination starts. If  $K \ll 1$  the RHNs never thermalize with the radiation bath as seen in Fig. 4 (**Left**). If  $K \gtrsim 1$ , the RHNs eventually thermalize with the radiation bath due to their strong Yukawa interactions with the SM particles as shown in Fig. 4 (**Right**).
3. *Case (c): Thermal leptogenesis* - For large enough  $y_R$  and for  $T_{N_1} \ll T_\phi$ , the RHNs

produced from  $\phi$  can quickly thermalize with the radiation bath and attain thermal abundance via 2-to-2 scattering process  $N_i N_i \leftrightarrow \phi \leftrightarrow \bar{f} f$  (see Appendix B for details). This scenario is similar to thermal leptogenesis. The scalar will decay to both RHNs and radiation that will usher in an era of radiation domination, with the RHNs contributing to the radiation. In general, RHNs will also be produced thermally from the radiation bath via the scattering process. After attaining thermal abundance, eventually the RHNs freeze-out when the scattering process decouples, and then decay at  $T_{N_1}$ . Depending on their decay widths, these RHNs may or may not dominate the energy density prior to its decay. We are interested in the scenario when they do dominate. The necessary condition for that is [61, 131],

$$T_{N_1} < T_{\text{dom}}^{N_1} \lesssim 2\% M_1 \quad (32)$$

which is the fermionic version of Eq. (25). The scalar dynamics adds nothing new to the final lepton asymmetry compared to the traditional thermal leptogenesis scenario. On the other hand, entropy injection now takes place in two stages: first at around  $T_\phi$  when  $\phi$  decays and secondly at RHN decay temperature  $T_{N_1}$ . Hence this case corresponds to 2-step entropy injection contrary to the non-thermal case, where entropy is injected in 1 step. A requirement for two-step entropy injection is,

$$T_\phi \gg T_{\text{dom}}^{N_1} \quad (33)$$

such that after their non-thermal production from  $\phi$ , RHNs get enough time to thermalize then freeze-out before they start to dominate.

### A. Analytical Estimates of Equilibrium Temperature

Equilibrium temperature is the temperature at which matter domination ends, kickstarting the latest radiation dominated era. From the discussion above and from Fig. 3 and Fig. 4, we see that it is around the decay temperatures  $T_\phi$  or  $T_{N_1}$  depending on which one is smaller,

$$T_{\text{dec.}} \sim \text{Min}[T_\phi, T_{N_1}] \quad (34)$$

We use this temperature in Eq. (48) for calculating the damped GW spectrum from inflation. Note that the exact equilibrium temperature is a little lower than the decay temperature

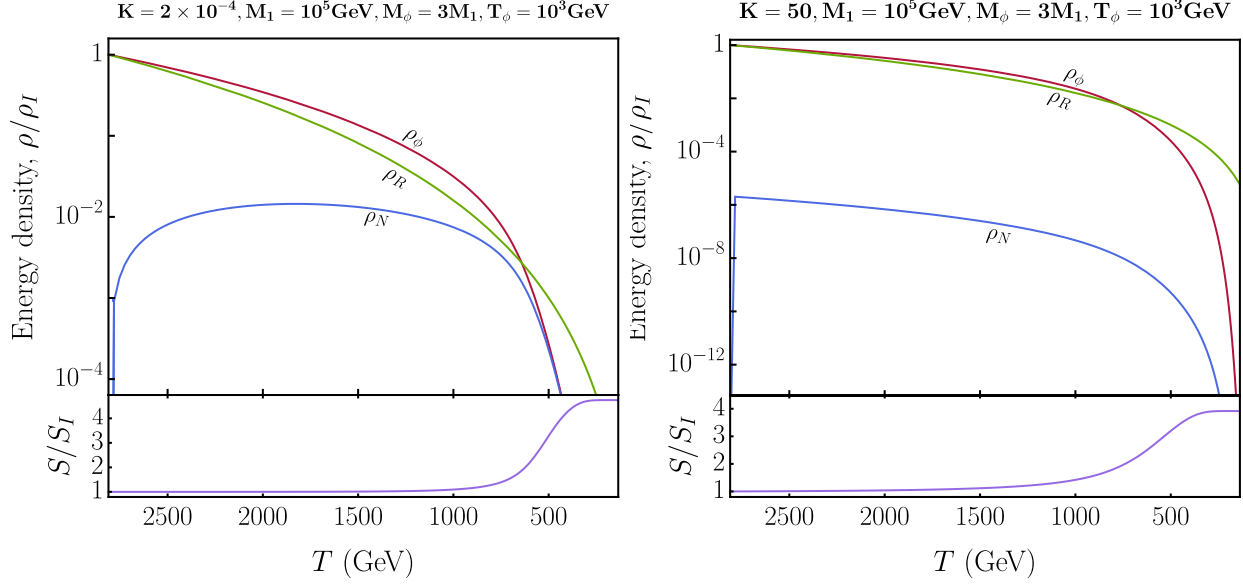


FIG. 3: The evolution of the energy densities of the scalar  $\rho_\phi$ , RHN  $\rho_N = \rho_{N_1} + \rho_{N_2}$  and radiation,  $\rho_R$  with respect to the radiation temperature. Here we have taken  $M_1 = 10^5$ ,  $M_\phi = 3M_1$ ,  $T_\phi = 10^3$  GeV for weak washout  $K = 2 \times 10^{-4}$  (**Left**) and strong washout  $K = 50$  (**Right**). Both correspond to Case (a) mentioned at the beginning of Sec. IV. We can see RHNs instantaneously decay after production. The bottom panels in each of the images show the amount of entropy injected,  $S = sa^3$  where  $s \propto T^3$  is the entropy density defined in Eq. (24) and  $a$  is the scale factor.

since the decay is not instantaneous. However for our considerations,  $T_{\text{dec.}}$  is a reasonable estimate of it.

If we have thermal RHN scenario discussed in Case (c) above, provided the RHNs dominate before decaying, there are two stages of entropy injection, one from scalar decay at  $T_\phi$  and another from RHN decay at  $T_{N_1}$ . In that case, we have an additional radiation dominated era between the two matter dominated epochs. Hence we take the two equilibrium temperatures to be  $T_\phi$  and  $T_{N_1}$  in this scenario.

## B. Dilution Factor from Entropy Injection

Both scalar and RHN decay injects entropy into the Universe if the decay products thermalize quickly with the radiation bath. The general formula for the dimensionless dilution

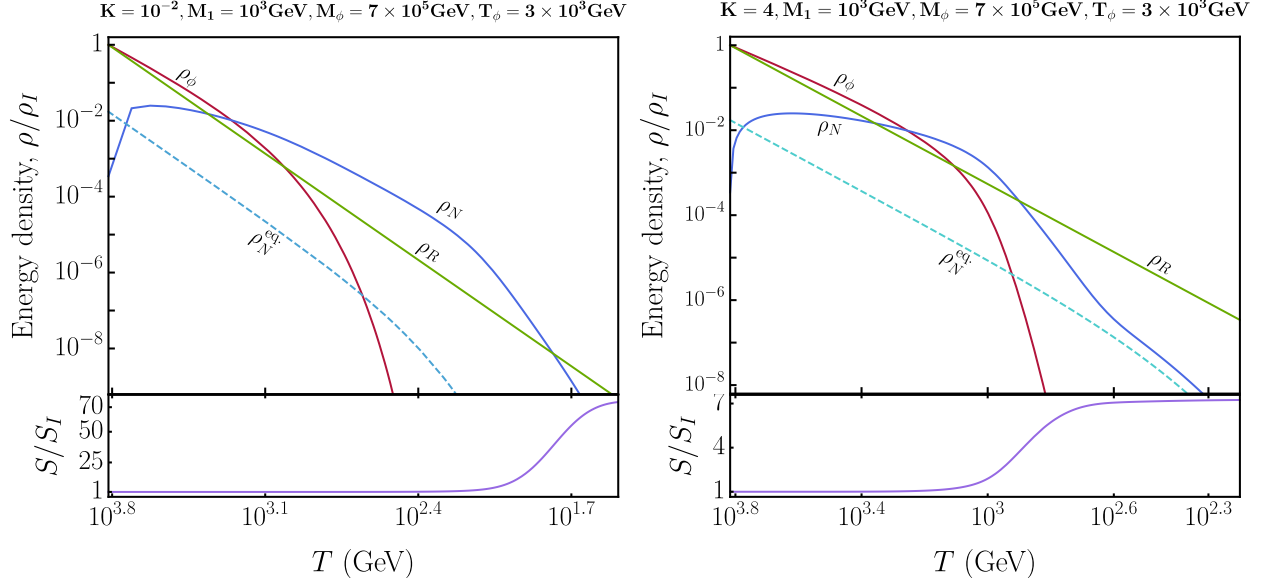


FIG. 4: Same as Fig. 3 but for RHN domination scenario, as described in Case (b) of Sec. IV.

For weak washout,  $K \ll 1$  (**Left**), RHNs are always out-of-equilibrium. For strong washout,  $K \gg 1$  (**Right**), RHNs get thermalized later due to their strong Yukawa interactions. The final asymmetry can be calculated numerically by solving the Boltzmann equations. The bottom panels show the entropy injection.

factor from the entropy injection by a dominating species  $\chi$  decaying to relativistic particles is given by [61, 96]

$$\Delta = \frac{s(T_{\text{after}})a^3(T_{\text{after}})}{s(T_{\text{before}})a^3(T_{\text{before}})} = \left( 1 + 2.95 \left( \frac{2\pi^2 \langle g_*(T) \rangle}{45} \right)^{\frac{1}{3}} \frac{(\frac{n_\chi}{s} M_\chi)^{\frac{4}{3}}}{(M_{\text{pl}} \Gamma_\chi)^{\frac{2}{3}}} \right)^{\frac{3}{4}} \quad (35)$$

where  $s$  is the entropy density,  $T_{\text{before/after}}$  represents temperature before/after the decay process and  $\frac{n_\chi}{s}$  is the initial abundance of the particle  $\chi$ .

For our analysis, we estimate the dilution factor using the formula in (35) for the 3 classifications we made:

*Case (a):* In this case, the RHNs decay out-of-equilibrium instantaneously to relativistic particles at  $T_\phi$ . Therefore we can assume that it is the scalar which is directly decaying to the radiation bath releasing entropy. The dilution factor  $\Delta$  can be given by Eq. (35) with  $\chi$  replaced by  $\phi$ . The initial abundance is given by Eq. (23). In the large entropy injection

approximation  $\Delta \gg 1$ , using Eq. (27) we can write the dilution factor to be,

$$\Delta \simeq 3.7 \times 10^9 \left( \frac{M_\phi}{10^{15} \text{ GeV}} \right) \left( \frac{\text{TeV}}{T_\phi} \right) \quad (36)$$

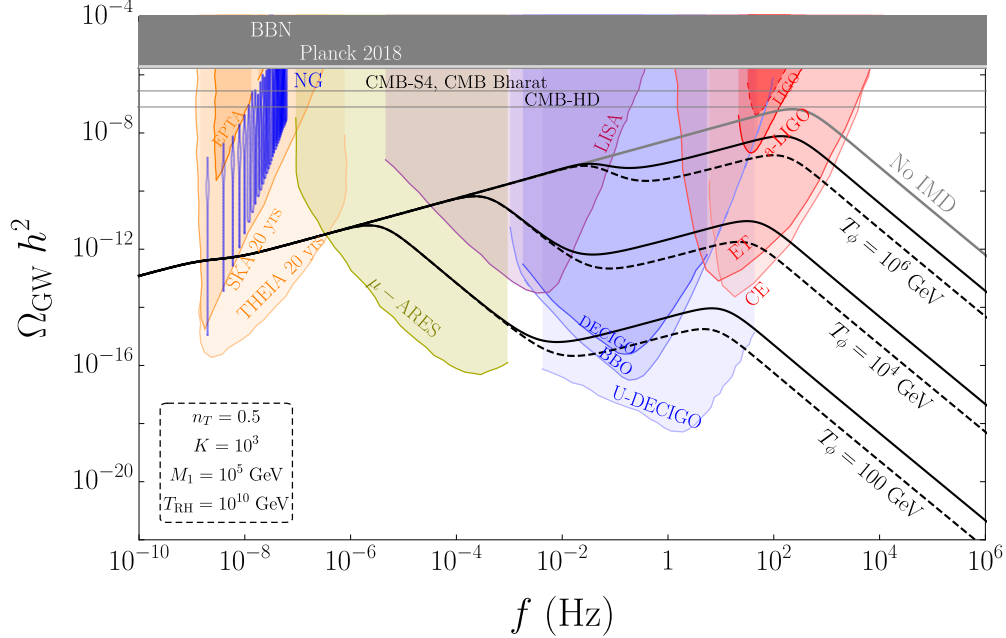


FIG. 5: *Suppressed gravitational spectra of a benchmark Case (a) scenario when RHNs decay instantaneously. Here we have taken  $r = 0.035$ ,  $n_T = 0.5$ ,  $T_{\text{RH}} = 10^{10} \text{ GeV}$ ,  $K = 10^3$ , and varied  $T_\phi$  and  $M_\phi$ . Gray line shows the standard GW spectrum without any intermediate matter domination. Black solid and dashed lines correspond to  $M_\phi = 10^9$  and  $3 \times 10^9 \text{ GeV}$  respectively. The extreme dampening at frequencies above  $\sim 10 \text{ Hz}$  is due to inflaton decay.*

*Case (b):* RHNs dominate the energy budget of the Universe as soon as they are produced. The energy density stored in  $\phi$  species is first transferred to the RHNs and then dumped into the radiation bath when RHNs decay at  $T_{N_1}$ . Hence, this scenario can be imagined as if  $\phi$  itself is decaying to SM particles at  $T_{N_1}$ .

The dilution factor in that case will be same as Case (a), except  $\Gamma_\phi$  will be replaced by  $\Gamma_{N_1}^{rf}$  in Eq. (35) to specify the elongated period of matter domination compared to Case (a). Note that considering only the lightest RHN  $N_1$  is sufficient here. Again in the large entropy injection limit  $\Delta \gg 1$ , one can write the dilution factor as,

$$\Delta \simeq 3.7 \times 10^9 \left( \frac{M_\phi}{10^{15} \text{ GeV}} \right) \left( \frac{10^5 \text{ GeV}}{M_1} \right) \sqrt{\frac{10^{-4}}{K}} \quad (37)$$

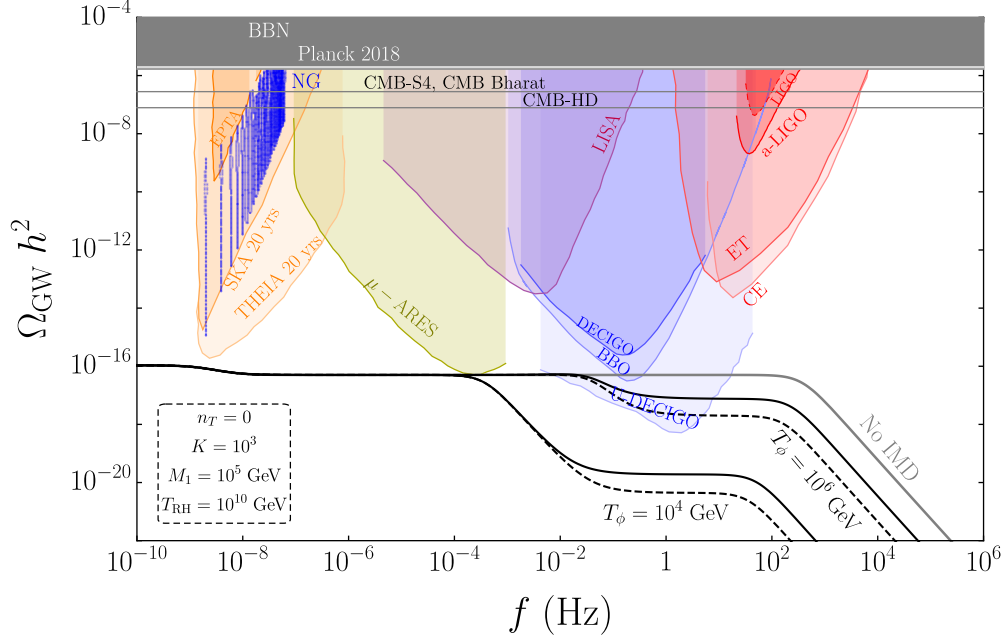


FIG. 6: Same as Fig. 5 but for  $n_T = 0$ . Solid and dashed black lines correspond to  $M_\phi = 10^9$  and  $3 \times 10^9$  GeV respectively.

*Case (c):* As discussed earlier, within suitable parameter choices, one can obtain thermal leptogenesis with two-step entropy injection (Appendix B). The dilution factor from scalar decay  $\Delta_\phi$  is again estimated by Eq. (36) as in Case (a), while the dilution factor for RHNs,  $\Delta_N$  is calculated assuming an initial RHN abundance just before their decay to be [98],

$$\frac{n_N}{s} = \frac{135 \zeta(3)}{4\pi^4 g_{*S}} \quad (38)$$

which is based on the assumption that RHNs were relativistic when they froze out, analogous to Eq. (23). In the large entropy injection limit  $\Delta_N$  is given as,

$$\Delta_N \simeq 1109 \sqrt{\frac{10^{-10}}{K}} \quad (39)$$

Lastly, if the RHNs do not dominate (see Eq. (32)), we only have 1-step entropy injection from scalar decay and corresponding dilution factor  $\Delta_\phi$ . In that case, GW experiments can not probe the leptogenesis scale, since no suppression of the inflationary GW spectrum occurs at  $T_{N_1}$ .

## V. GRAVITATIONAL WAVES OF INFLATIONARY ORIGIN

### A. Primordial spectrum in standard and non-standard cosmology

Primordial inflation, the early exponential expansion of the Universe, is believed to have transitioned into an epoch known as reheating. This transition resulted in the creation of a high-energy plasma of radiation, following the dynamics of the Standard Model of particle physics. During inflation, gravitational waves (GWs) from quantum tensor fluctuations of the metric were generated. Initially, while outside the cosmological horizon, these GWs exhibited constant amplitudes. However, as they re-entered the horizon in the radiation-dominated era, their amplitudes underwent damping. The propagation of GW modes that re-enter the horizon is controlled by a transfer function.

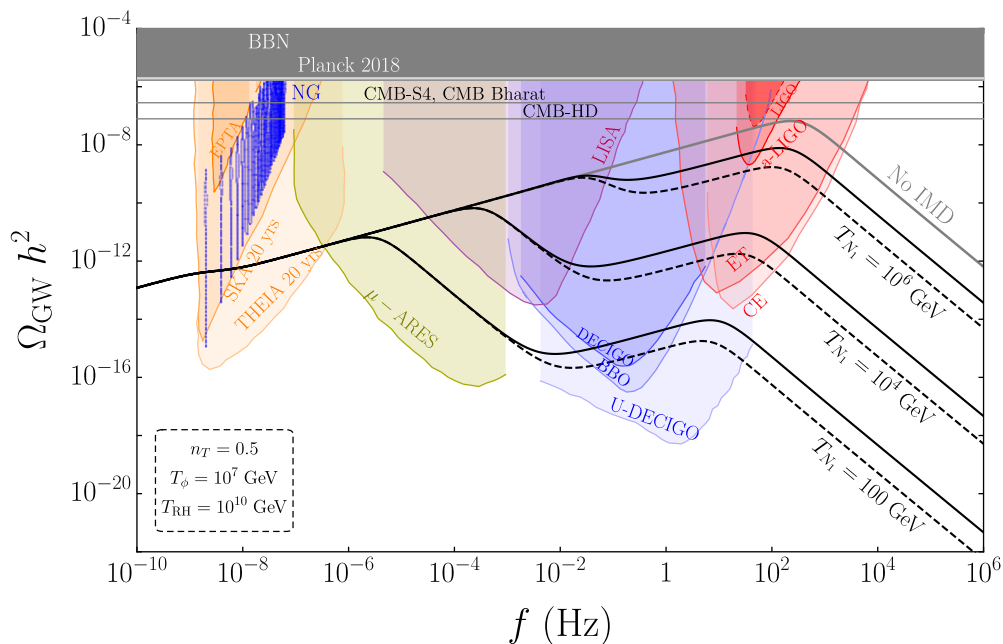


FIG. 7: Same as Fig. 5 but for a benchmark Case (b), “RHN domination” scenario. Here we take  $T_\phi = 10^7$  GeV,  $r = 0.035$ ,  $n_T = 0.5$  and vary the washout parameter  $K$  along with  $M_1$  and  $M_\phi$ . The spectral shape depends on the leptogenesis scale  $T_{N_1} = M_1 \sqrt{K}$  as shown. Again, solid and dashed black lines represent  $M_\phi = 10^9$  and  $3 \times 10^9$  GeV respectively.

The current power spectrum of GWs, denoted as  $\Omega_{\text{GW}}(k)$  can be expressed as a function of the wave number,  $k = 2\pi f$  where  $f$  is the frequency [61],

$$\Omega_{GW}(k) = \frac{1}{12} \left( \frac{k}{a_0 H_0} \right)^2 T_T^2(k) P_T^{\text{prim.}}(k) \quad (40)$$

with  $a_0 = 1$  representing the present-day scale factor and  $H_0 \approx 2.2 \times 10^{-4} \text{ Mpc}^{-1}$  being the current Hubble expansion rate [119].  $P_T^{\text{prim.}}(k)$  is the primordial tensor power spectrum from inflation, and  $T_T^2(k)$  is the transfer function that characterizes the propagation of GWs in the background of a Friedmann-Lemaitre-Robertson-Walker (FLRW) Universe after the temperature at the time of horizon re-entry,  $T_{\text{in}}$  given by [88]:

$$T_{\text{in}} = 5.8 \times 10^6 \text{ GeV} \left( \frac{106.75}{g_*(T_{\text{in}})} \right)^{1/6} \left( \frac{k}{10^{14} \text{ Mpc}^{-1}} \right) \quad (41)$$

The conventional parameterization for the inflationary tensor power spectrum,  $P_T^{\text{prim.}}(k)$  typically involves expressing its amplitude ( $A_T$ ) and spectral index ( $n_T$ ) with respect to the pivot scale  $k_* = 0.05 \text{ Mpc}^{-1}$ , as outlined in the Planck 2018 analysis [132].

$$P_T^{\text{prim.}}(k) = A_T(k_*) \left( \frac{k}{k_*} \right)^{n_T} \quad (42)$$

where the amplitude  $A_T(k_*)$  is related to the scalar power spectrum via the tensor-to-scalar-ratio  $r \leq 0.035$  [133]:

$$A_T(k_*) = A_S(k_*) r, \quad A_S(k_*) = 2.0989 \times 10^{-9} \quad (43)$$

where  $A_S(k_*)$  is scalar power spectrum [132]. For our analysis we fix the value of  $r = 0.035$ . The spectral index  $n_T$  plays a critical role in characterizing the inflationary tensor power spectrum. While standard single-field slow-roll inflation predicts a red-tilted spectrum, where  $n_T$  satisfies the consistency relation  $n_T = -r/8$  [134], other scenarios, including blue-tilted spectra ( $n_T > 0$ ), are well-motivated in various cosmological models [135–142].

Numerical computation and analytical fitting gives the transfer function  $T_T^2(k)$  as:

$$T_T^2(k) = \Omega_m^2 \left( \frac{g_*(T_{\text{in}})}{g_*^0} \right) \left( \frac{g_{*S}^0}{g_{*S}(T_{\text{in}})} \right)^{4/3} \left( \frac{3j_1(z_k)}{z_k} \right)^2 F(k) \quad (44)$$

Here,  $g_*^0 = 3.36$  and  $g_{*S}^0 = 3.91$  are the present-day values of the effective degrees of freedom.  $\Omega_m = 0.31$  [119] is the total matter density. The Bessel function  $j_1(z_k)$  describes the damping of GW amplitudes after horizon re-entry with  $z_k \equiv k\tau_0$  and  $\tau_0 = 2/H_0$ . In the limit  $z_k \gg 1$ , relevant for the frequencies of interest, we can replace  $j_1(z_k)$  for  $1/(\sqrt{2}z_k)$ . Finally, the

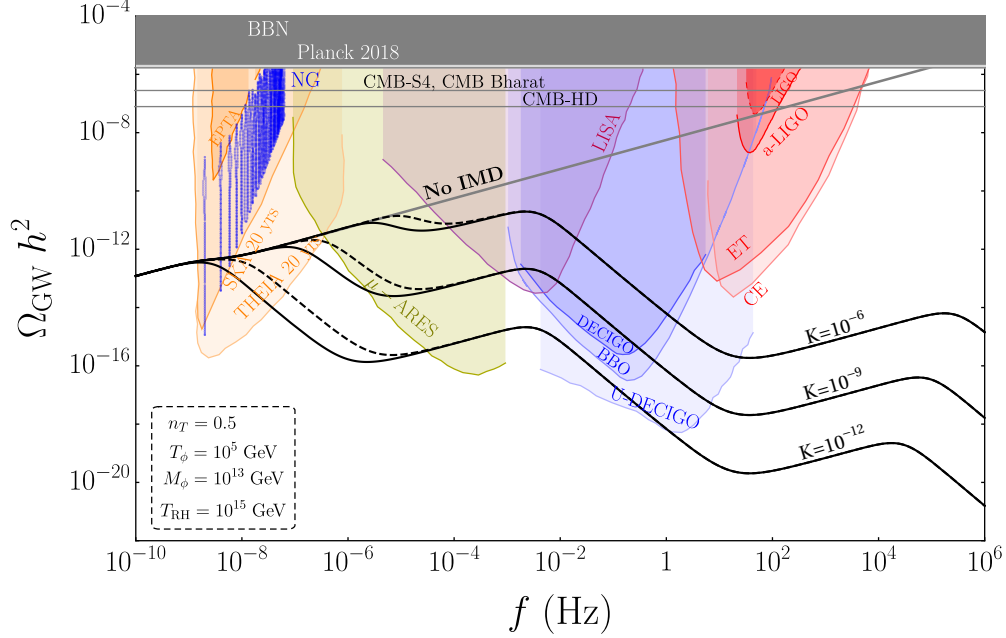


FIG. 8: Same as Fig. 5 but for Case (c), thermal leptogenesis, portraying 2-step entropy injection and a knee-like feature around  $f \sim 10^{-2}$  Hz due to  $\phi$  decay, in addition to the one due to RHN decay at lower frequencies. Here, we take  $r = 0.035$ ,  $n_T = 0.5$ ,  $M_\phi = 10^{13}$  GeV,  $T_\phi = 10^5$  GeV and  $R_{\text{RH}} = 10^{15}$  GeV. The effect of  $K$  is shown. The solid and dashed line correspond to  $M_1 = 10^5$  and  $3 \times 10^5$  GeV.

fitting function  $F(k)$  in standard cosmology is given by [143],

$$F(k)_{\text{standard}} = T_1^2 \left( \frac{k}{k_{\text{eq.}}} \right) T_2^2 \left( \frac{k}{k_{\text{RH}}} \right) \quad (45)$$

If there was an intermediate matter domination epoch, the fitting function is modified [143],

$$F(k)_{\text{IMD}} = T_1^2 \left( \frac{k}{k_{\text{eq.}}} \right) T_2^2 \left( \frac{k}{k_{\text{dec.}}} \right) T_3^2 \left( \frac{k}{k_{\text{dec. S}}} \right) T_2^2 \left( \frac{k}{k_{\text{RH S}}} \right) \quad (46)$$

Here we introduce:

$$k_{\text{eq.}} = 7.1 \times 10^{-2} \text{ Mpc}^{-1} \cdot \Omega_m h^2 \quad (47)$$

$$k_{\text{dec.}} = 1.7 \times 10^{14} \text{ Mpc}^{-1} \left( \frac{g_{*S}(T_{\text{dec.}})}{g_{*S}^0} \right)^{1/6} \left( \frac{T_{\text{dec.}}}{10^7 \text{ GeV}} \right) \quad (48)$$

$$k_{\text{RH}} = 1.7 \times 10^{14} \text{ Mpc}^{-1} \left( \frac{g_{*S}(T_{\text{RH}})}{g_{*S}^0} \right)^{1/6} \left( \frac{T_{\text{RH}}}{10^7 \text{ GeV}} \right) \quad (49)$$

$$k_{\text{dec. S}} = k_{\text{dec.}} \Delta^{2/3} \quad (50)$$

$$k_{\text{RH S}} = k_{\text{RH}} \Delta^{-1/3} \quad (51)$$

where  $T_{\text{dec.}}$  is defined by (34) and we set  $h = 0.7$ . The entropy dilution factor  $\Delta$  is the dilution factor and the fit functions read,

$$T_1^2(x) = 1 + 1.57x + 3.42x^2 \quad (52)$$

$$T_2^2(x) = (1 - 0.22x^{3/2} + 0.65x^2)^{-1} \quad (53)$$

$$T_3^2(x) = 1 + 0.59x + 0.65x^2 \quad (54)$$

At this point we can plot the spectrum  $\Omega_{\text{GW}} h^2$  as a function of current frequency, using Eq. (40). We discuss the features in these plots accounting for  $\phi$  and  $N$  domination in Sec. VI A. The suppression of the GW spectrum happens above a frequency  $f_{\text{sup}}$ , given by,

$$f_{\text{sup}} \simeq 2.7 \times 10^{-8} \text{ Hz} \left( \frac{T_{\text{dec.}}}{\text{GeV}} \right) \quad (55)$$

The suppression factor is given by [77],

$$R_{\text{sup}} = \frac{\Omega_{\text{GW}}^{\text{IMD}}}{\Omega_{\text{GW}}^{\text{standard}}} \simeq \frac{1}{\Delta^{4/3}} \quad (56)$$

## B. Two-step entropy injection

Our Case (c) discussed in Sec. IV has two stages of entropy injection. We propose a modified transfer function to incorporate the two stages along the lines of [143], by assuming the form of the fitting function to be,

$$F(k)_{\text{IMD}}^{2\text{-step}} = T_1^2 \left( \frac{k}{k_{\text{eq.}}} \right) T_2^2 \left( \frac{k}{k_{\text{dec.}}^\phi} \right) T_3^2 \left( \frac{k}{k_{\text{dec. S}}^\phi} \right) T_2^2 \left( \frac{k}{k_{\text{dec.}}^N} \right) T_3^2 \left( \frac{k}{k_{\text{dec. S}}^N} \right) T_2^2 \left( \frac{k}{k_{\text{RH S}}^{2\text{-step}}} \right) \quad (57)$$

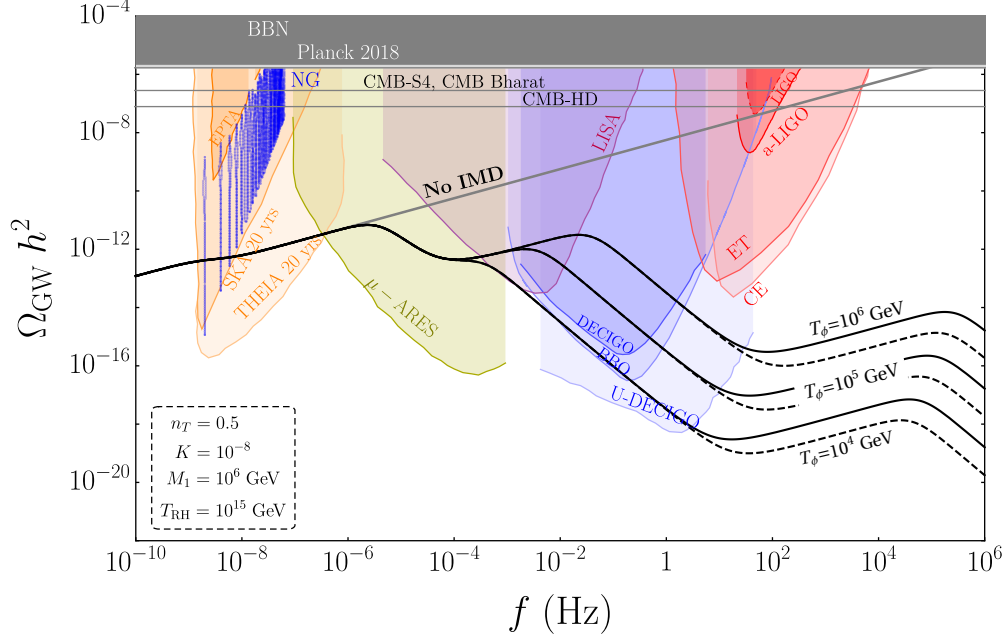


FIG. 9: Same as Fig. 8 but here we take  $M_1 = 10^6$  GeV,  $K = 10^{-8}$  and show the dependence of the spectral shape on  $T_\phi$  and  $M_\phi$ . The solid and dashed lines represent  $M_\phi = 10^{13}$  and  $3 \times 10^{13}$  GeV respectively.

where  $k_{\text{dec.}}^\phi, k_{\text{dec.}}^N$  are related to the decay temperatures  $T_\phi$  and  $T_{N_1}$  respectively and  $k_{\text{dec.S}}^\phi, k_{\text{dec.S}}^N$  are related to the domination temperatures of  $\phi$  and  $N_1$  respectively. We define them as,

$$k_{\text{dec.}}^\phi = 1.7 \times 10^{14} \text{ Mpc}^{-1} \left( \frac{g_{*S}(T_\phi)}{g_{*S}^0} \right)^{1/6} \left( \frac{T_\phi}{10^7 \text{ GeV}} \right) \quad (58)$$

$$k_{\text{dec.}}^N = 1.7 \times 10^{14} \text{ Mpc}^{-1} \left( \frac{g_{*S}(T_{N_1})}{g_{*S}^0} \right)^{1/6} \left( \frac{T_{N_1}}{10^7 \text{ GeV}} \right) \quad (59)$$

$$k_{\text{dec.S}}^\phi = k_{\text{dec.}}^\phi \Delta_\phi^{2/3} \quad (60)$$

$$k_{\text{dec.S}}^N = k_{\text{dec.}}^N \Delta_N^{2/3} \quad (61)$$

$$k_{\text{RH S}}^{2\text{-step}} = k_{\text{RH}} (\Delta_\phi \Delta_N)^{-1/3} \quad (62)$$

where  $\Delta_\phi, \Delta_N$  are the dilution factors from  $\phi$  and RHN decays respectively. The necessary conditions to use this transfer function are  $M_\phi \gg M_1, T_\phi > T_{N_1}$  and Eq. (32) as discussed earlier. A proper way to obtain the 2-step transfer function requires numerical fitting which we left as a future direction. In this case we have two suppression frequencies corresponding

to scalar and RHN decays, analogous to Eq. (55),

$$f_{\text{sup}}^{\phi} \simeq 2.7 \times 10^{-8} \text{ Hz} \left( \frac{T_{\phi}}{\text{GeV}} \right), \quad f_{\text{sup}}^N \simeq 2.7 \times 10^{-8} \text{ Hz} \left( \frac{T_{N_1}}{\text{GeV}} \right), \quad (63)$$

And similar to Eq. (56), the suppression factors corresponding to the first ( $\phi$  decay) and the second ( $N$  decay) step of entropy injection are given by,

$$R_{\text{sup}}^{\text{1st}} \simeq \frac{1}{(\Delta_{\phi} \Delta_N)^{4/3}}, \quad R_{\text{sup}}^{\text{2nd}} \simeq \frac{1}{\Delta_N^{4/3}} \quad (64)$$

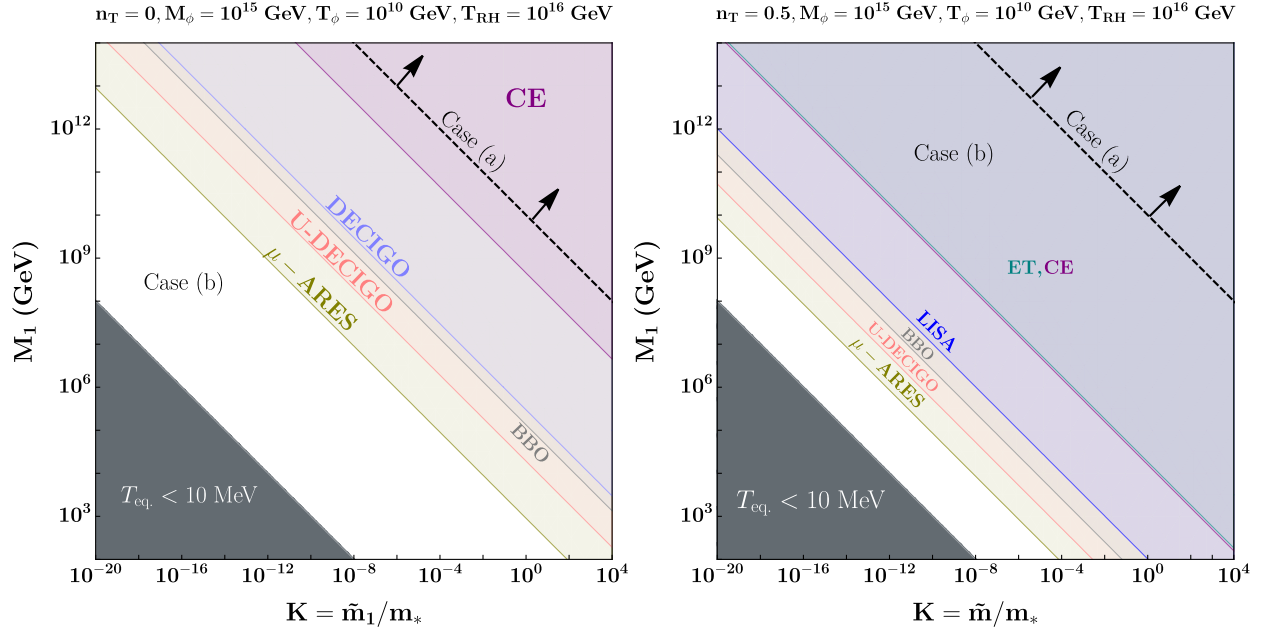


FIG. 10: *Projected sensitivities of different experiments in the RHN parameter space for  $n_T = 0$  (Left) and  $n_T = 0.5$  (Right). Here  $\tilde{m}_1$  is the effective neutrino mass defined by Eq. (8) and  $m_* = 1.1 \times 10^{-3} \text{ eV}$  is the equilibrium neutrino mass defined in Eq. (9). For both plots we took  $M_{\phi} = 10^{15} \text{ GeV}$ ,  $T_{\phi} = 10^{10} \text{ GeV}$ ,  $r = 0.035$ . The colored regions associated with each experiment implies sensitivity with  $\text{SNR} > 10$ . As expected, a higher  $n_T$  increases overall SNR. See main text for detailed description and analysis.*

### C. Signal-to-noise ratio (SNR)

Interferometers are instruments that measure displacements in terms of dimensionless strain-noise denoted as  $h_{\text{GW}}(f)$ . This strain-noise is related to the amplitude of gravitational waves (GWs) and can be converted into an energy density, expressed by the formula:

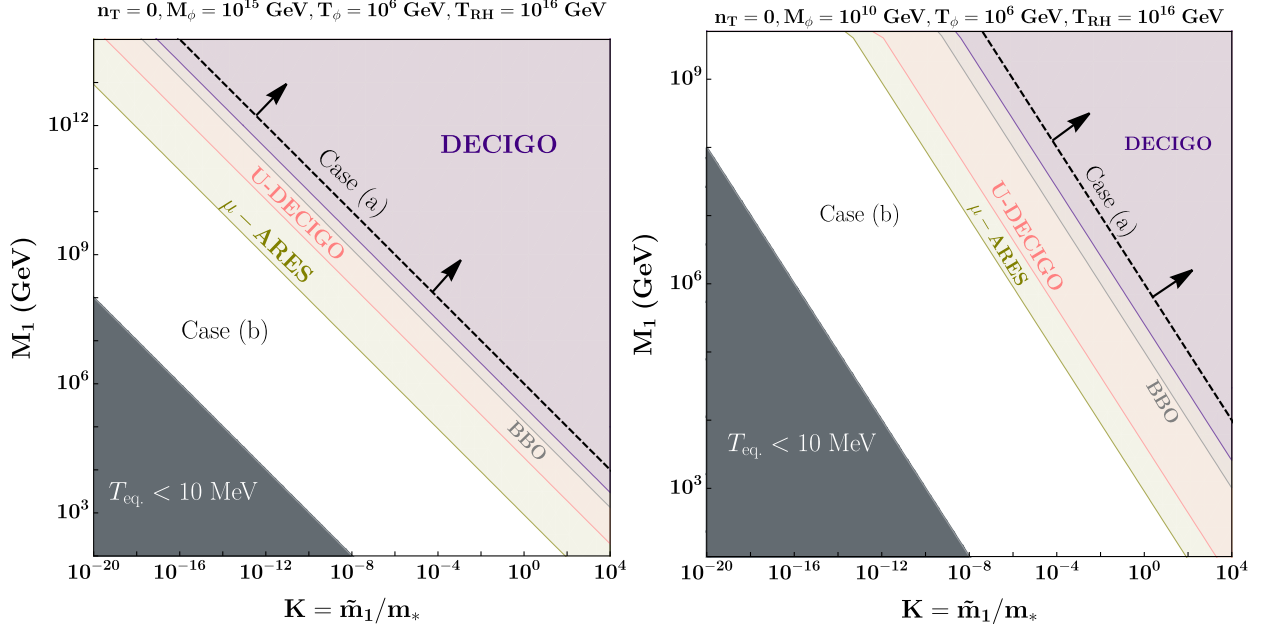


FIG. 11: Same as Fig. 10 but for  $n_T = 0$ ,  $T_\phi = 10^6 \text{ GeV}$  and  $M_\phi = 10^{15} \text{ GeV}$  (**Left**) and  $10^{10} \text{ GeV}$  (**Right**). For a fixed  $T_\phi$ , the left plot is expected to have smaller overall SNR values due to higher  $M_\phi$ . Here  $m_* = 1.1 \times 10^{-3} \text{ eV}$ .

$$\Omega_{\text{exp}}(f)h^2 = \frac{2\pi^2 f^2}{3H_0^2} h_{\text{GW}}(f)^2 h^2 \quad (65)$$

Here,  $H_0$  represents the present-day Hubble rate ( $H_0 = h \times 100 \frac{\text{km/s}}{\text{Mpc}}$ ). To assess the likelihood of detecting the primordial GW background, we calculate the signal-to-noise ratio (SNR) using the experimental sensitivity  $\Omega_{\text{exp}}(f)h^2$ , either given or projected. The SNR is determined by the following formula:

$$\text{SNR} \equiv \sqrt{\tau} \int_{f_{\text{min}}}^{f_{\text{max}}} df \left( \frac{\Omega_{\text{GW}}(f)h^2}{\Omega_{\text{exp}}(f)h^2} \right)^2 \quad (66)$$

In this analysis, we use  $h = 0.7$  and an observation time of  $\tau = 4$  years. A detection threshold of  $\text{SNR} \geq 10$  is applied.

In the spectrum plots we display the sensitivity curves for different ongoing and future GW experiments. They can be grouped as:

- **Ground-based interferometers:** These detectors, such as LIGO/VIRGO [40, 41, 144–147], aLIGO/aVIRGO [148–150], AION [151–154], EINSTEIN TELESCOPE

(ET) [155, 156], and COSMIC EXPLORER (CE) [157, 158], use interferometric techniques on the Earth’s surface to detect gravitational waves.

- **Space-based interferometers:** Space-based detectors like LISA [159], BBO [160–162], DECIGO, U-DECIGO [163, 164], AEDGE [151, 165], and  $\mu$ -ARES [166] are designed to detect gravitational waves from space, offering different advantages over ground-based counterparts.
- **Recasts of star surveys:** Surveys such as GAIA/THEIA [167] utilize astrometric data from stars to indirectly infer the presence of gravitational waves.
- **Pulsar timing arrays (PTA):** PTA experiments like SKA [42–44], EPTA [45, 46], and NANOGrAV [168–170] use precise timing measurements of pulsars to detect gravitational wave signatures.
- **CMB polarization:** Experiments like Planck 2018 [14, 132], BICEP 2/Keck [133] as computed by [171], and LITEBIRD [172] focus on detecting gravitational wave imprints in the polarization of the cosmic microwave background radiation.
- **CMB spectral distortions:** Projects like PIXIE, SUPER-PIXIE [173], and VOYAGER2050 [174] aim to detect gravitational wave signatures through spectral distortions in the cosmic microwave background.

The blue violine lines in the spectrum plots are the most recent data from NANOGrav.

#### D. Bounds from BBN and CMB on dark radiation

The gravitational wave energy density should be smaller than the bound on dark radiation parameterized as the number of additional neutrinos  $\Delta N_{\text{eff}}$  [175, 176],

$$\int_{f_{\text{min}}}^{\infty} \frac{df}{f} \Omega_{\text{GW}}(f) h^2 \leq 5.6 \times 10^{-6} \Delta N_{\text{eff}} \quad (67)$$

We neglect the frequency dependence of this bound and set  $\Omega_{\text{GW}} \leq 5.6 \times 10^{-6} \Delta N_{\text{eff}}$  for the GW spectra that we calculate. BBN puts a bound on  $\Delta N_{\text{eff}}^{\text{BBN}} \simeq 0.4$  [177]. Planck plus BAO observations set the bound  $\Delta N_{\text{eff}}^{\text{Planck+BAO}} \simeq 0.28$  [14]. Projected bounds from future experiments are  $\Delta N_{\text{eff}}^{\text{Proj.}} = 0.014$  for CMB-HD [178],  $\Delta N_{\text{eff}}^{\text{Proj.}} = 0.05$  for CMB-Bharat [179],

$\Delta N_{\text{eff}}^{\text{Proj.}} = 0.06$  for CMB Stage IV [180] and NASA’s PICO mission [181],  $\Delta N_{\text{eff}}^{\text{Proj.}} \lesssim 0.12$  for CORE [182], the South Pole Telescope [183] and Simons observatory [184].

## VI. RESULTS

### A. Example spectra for different cases

Fig. 5 illustrates the damped gravitational wave (GW) spectra for Case (a) discussed in Sec. IV, assuming spectral index  $n_T = 0.5$  and  $r = 0.035$ , demonstrating the influence of  $T_\phi$  and  $M_\phi$ , alongside sensitivity curves of current and future GW experiments. The blue violin lines are taken from recent NANOGrav 15yr dataset [47, 48]. Different horizontal lines on the plot are coming from the current or projected  $\Delta N_{\text{eff}}$  bounds from BBN, Planck 2018 and CMB surveys [61]. In Case (a) scenario, characterized by the condition  $T_\phi < T_{N_1}$ , we set the minimum  $T_\phi$  to be approximately 100 GeV to accommodate sphaleron effects within the electroweak scale. The gray solid line marked “No IMD” is the standard spectrum with no intermediate matter dominated phase while the black solid and dashed lines are the spectral shapes in presence of the matter dominated epoch. Higher frequencies in the figure correspond to earlier times, showcasing suppression beyond the critical frequency  $f_{\text{sup}}$  due to entropy injection given by Eq. (55). Suppression at frequencies higher than  $f_{\text{sup}} \sim 10^{-5} - 0.1$  Hz are attributed to scalar and right-handed neutrino (RHN) decay, while suppression beyond  $\sim 10$  Hz is a consequence of inflaton decay terminating at the reheating temperature  $T_{\text{RH}} = 10^{10}$  GeV. Lower values of  $T_\phi$  shift the suppression frequency to the left and increase dilution factor. The solid and dashed spectral lines represent  $M_\phi = 10^9$  and  $3 \times 10^9$  GeV respectively. A higher  $M_\phi$  means more dilution. Importantly, GW signatures remain invariant across weak and strong washout regimes, as they solely depend on the scalar dynamics in this case. Fig. 6 is same as Fig. 5 but shown for  $n_T = 0$ .

Fig. 7 presents the GW signature of long-lived RHNs in Case (b) for different values of the washout parameter  $K$  and lightest RHN mass  $M_1$ . Once again the solid and dashed spectral lines correspond to  $M_\phi = 10^9$  and  $3 \times 10^9$  GeV respectively. We choose the combination  $T_{N_1} = M_1 \sqrt{K}$  in a way such that  $100 \text{ GeV} \leq T_{N_1} < T_\phi$ , where we have taken  $T_\phi = 10^7$  GeV. Other parameters are set as:  $r = 0.035, n_T = 0.5, T_{\text{RH}} = 10^{10}$  GeV. We see that the role of  $T_\phi$  seen in Fig. 5 is taken up by  $T_{N_1}$  in this case, as expected.

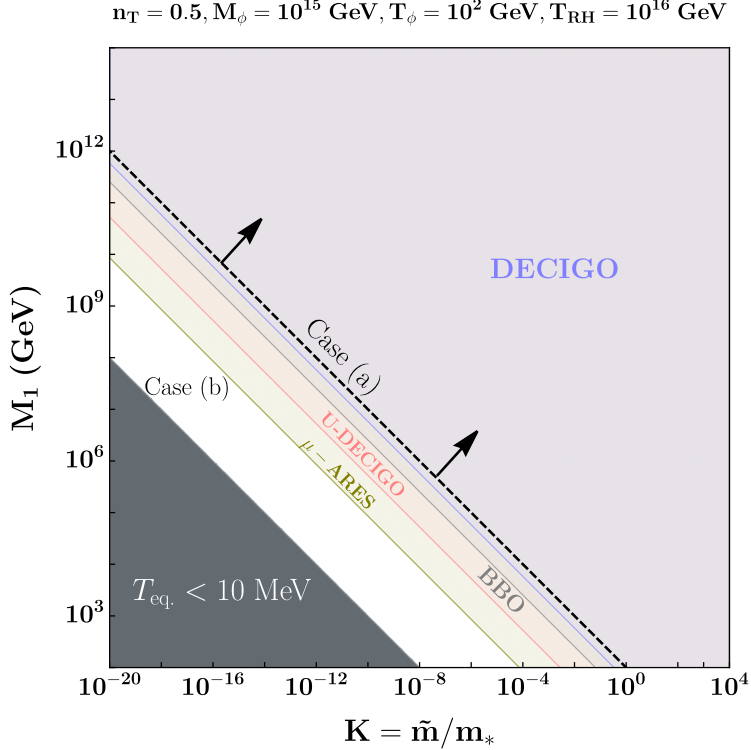


FIG. 12: Same as Fig. 10 but for  $T_\phi = 100 \text{ GeV}$  and  $n_T = 0.5$ ,  $M_\phi = 10^{15} \text{ GeV}$ . Here

$$m_* = 1.1 \times 10^{-3} \text{ eV}.$$

Case (c) mirrors thermal leptogenesis along with 2-step entropy injection as discussed earlier. Figures 8 and 9 depict the GW signatures of this scenario. For these plots, we make sure that the thermalization condition given in Eq. (B7) is satisfied assuming  $y_{N_i} = y_R$ , such the two-step entropy injection scenario is applicable. We use the 2-step transfer function utilizing Eq. (57). Notably, the scalar's effect manifests as an additional dip in the spectrum, a knee-like feature, positioned between the dips induced by inflaton decay and RHN decay. Thus we have two knee-like features, one from  $\phi$  decay and another from RHN decay. In Fig. 8 we show the dependency of the spectral shape on  $M_1$  and  $K$ , fixing  $T_\phi = 10^5 \text{ GeV}$ ,  $M_\phi = 10^{13} \text{ GeV}$ ,  $T_{\text{RH}} = 10^{15} \text{ GeV}$  for  $n_T = 0.5$ . The solid and dashed lines correspond to  $M_1 = 10^5$  and  $3 \times 10^5 \text{ GeV}$  respectively. Note that for  $T_{N_1} < 100 \text{ GeV}$ , efficient leptogenesis is not possible as sphalerons are turned off.

Finally in Fig. 9, we show the dependency of the spectrum on  $T_\phi$  and  $M_\phi$  fixing  $M_1 = 10^6 \text{ GeV}$ ,  $K = 10^{-8}$  such that leptogenesis scale is  $T_{N_1} = 100 \text{ GeV}$ . Other parameters are same as in Fig. 8. The solid and dashed lines here represent  $M_\phi = 10^{13}$  and  $3 \times 10^{13} \text{ GeV}$  respectively. The entropy injection from scalar is independent of leptogenesis scale but it

reduces the projected SNR for different experiments via the additional suppression as seen in the plots.

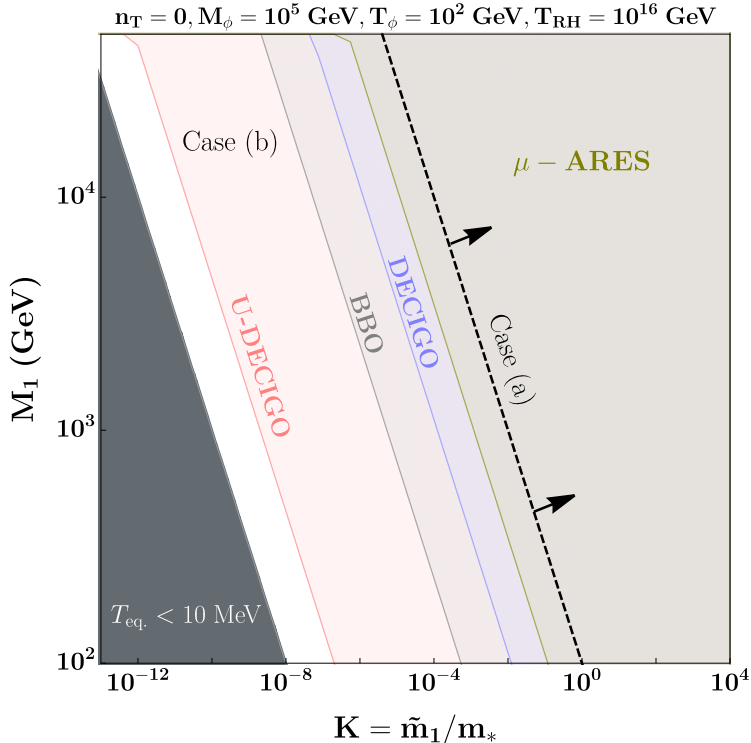


FIG. 13: Same as Fig. 10 but for  $T_\phi = 100$  GeV and  $n_T = 0$ ,  $M_\phi = 10^5$  GeV. Here  $m_* = 1.1 \times 10^{-3}$  eV.

## B. Estimates for Signal to Noise Ratio

The next set of Figures 10, 11, 12, 13, 14, 15 demonstrates the projected future sensitivities of U-DECIGO, DECIGO, BBO,  $\mu$ -ARES, LISA, CE and ET experiments in terms of signal to noise ratio (SNR) given in Eq. (66), in the parameter space of the RHN for different values of  $n_T$ ,  $M_\phi$ ,  $T_\phi$ ,  $T_{RH}$ . Figures 10, 11, 12, 13 correspond to non-thermal leptogenesis with black dashed line separating the Case (a) and Case (b) regions. Figures 14 and 15 demonstrate the thermal leptogenesis with two-step entropy injection scenario, Case (c), with green region specifying Case (a) and brown region corresponding to  $T_\phi < T_{\text{dom}}^{N_1}$ , where two-step entropy injection is not possible as described in Sec IV.

The gray shaded region is excluded from the requirement that  $T_{\text{eq}}$  should be larger than the BBN temperature of a few MeV. In Fig. 14 and 15 we are not interested in

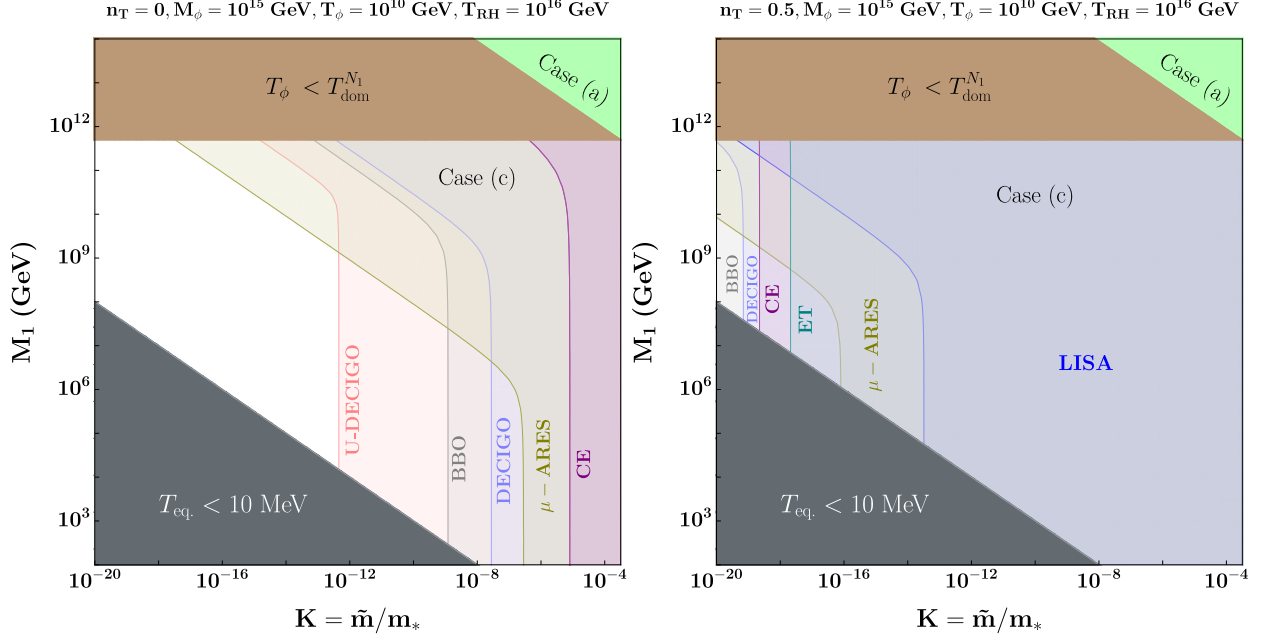


FIG. 14: Same as Fig. 10 but demonstrating thermal leptogenesis (Case (c) in Sec. IV) with two-step entropy injection for  $n_T = 0$  (Left) and  $n_T = 0.5$  (Right). Here  $m_* = 1.1 \times 10^{-3}$  eV.

For both plots we took  $M_\phi = 10^{15}$  GeV,  $T_\phi = 10^{10}$  GeV,  $r = 0.035$ . The green shaded region represents instantaneous RHN decay (Case (a)). Two-step entropy injection is not possible in the brown shaded region as  $T_\phi$  is less than RHN domination temperature  $T_{\text{dom}}^{N_1} \sim 2\% M_1$ . See main text for detailed description and analysis.

$K \gtrsim 10^{-4}$  where RHN domination is not possible, i.e. Eq. (32) is not satisfied, thus GW is not connected to leptogenesis in this region. In all the SNR plots, the colored regions associated with different experiments can be probed by that experiment with  $\text{SNR} \geq 10$ . In all these SNR plots we choose  $T_{\text{RH}} = 10^{16}$  GeV in order to eliminate its effect on the SNR. In vanilla leptogenesis scenario, vacuum stability of SM Higgs gives an upper bound on the lightest RHN mass  $M_1 \lesssim 10^{14}$  GeV [185, 186] and we assume it would be approximately the same in our model [54]. Hence we take upper limit on  $M_1$  to be around  $10^{14}$  GeV. On the other hand, the perturbativity limit of the model requires the Yukawa couplings  $\lambda_{ij} < 4\pi$ , which along with the necessity to produce at least one mass eigenstate  $m_\nu = 0.05$  eV gives another bound,  $M_2 \lesssim 10^{15}$  GeV. Hence, in our quasi-degenerate RHN model, we find the perturbativity bound  $M_1 \lesssim 10^{15}$  GeV. The perturbativity limit of the light-heavy neutrino mixing  $y_{N_i} < 4\pi$  is always satisfied in our model.

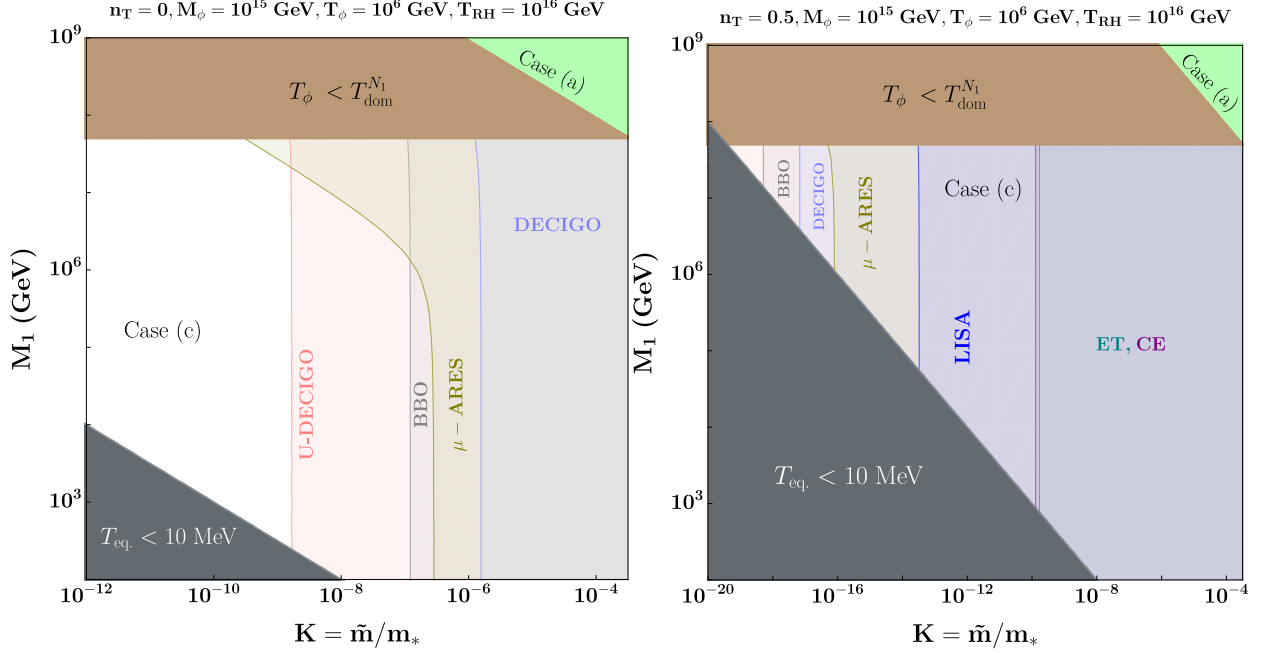


FIG. 15: Same as Fig. 14 but for  $T_\phi = 10^6$  GeV.

In Fig. 10, we pick a high scalar mass and decay temperature  $M_\phi = 10^{15}$  GeV,  $T_\phi = 10^{10}$  GeV and show the projected sensitivities of different experiments for  $n_T = 0$  (**Left**) and  $n_T = 0.5$  (**Right**). We see that increasing the spectral index  $n_T$  also increases the GW sensitive region by increasing the SNR as expected. For  $n_T = 0$ , LISA and ET will not be able to probe leptogenesis but for  $n_T = 0.5$  both the experiments will be sensitive to a large portion of the parameter space. In the Case (a) region of instantaneous RHN decay, the SNR will not depend on  $M_1$  and  $K$  but only on  $M_\phi$  and  $T_\phi$ . In the Case (b) region, RHNs decay at  $T_{N_1} = M_1 \sqrt{K}$ . Hence decreasing  $M_1$  or  $K$  results in more suppression and lower SNR.

In Fig. 11, we show the sensitivities for  $n_T = 0$ ,  $T_\phi = 10^6$  GeV and  $M_\phi = 10^{15}$  GeV (**Left**) and  $10^{10}$  GeV (**Right**). Both the left and right plots show almost the same sensitive area in the parameter space but suppression in the left plot is expected to be higher due to higher mass scalar decay. In both the plots we see the Case (a) region covering more space due to lower  $T_\phi$  value compared to Fig. 10. We also notice that CE is no longer sensitive for  $n_T = 0, T_\phi = 10^6$  GeV in Fig. 11 (**Left**) while it is sensitive for  $T_\phi = 10^{10}$  GeV in Fig. 10 (**Left**).

In Fig. 12, we show the effect of a low scalar decay temperature  $T_\phi = 100$  GeV assuming  $M_\phi = 10^{15}$  GeV. We note that lowering  $T_\phi$  increases the area of the region of instantaneous RHN decay (Case (a)) in the parameter space, and for  $n_T = 0.5$  most of the parameter space is accessible to DECIGO, BBO,  $\mu$ -ARES and U-DECIGO. We find no experiment to be sensitive to leptogenesis for  $n_T = 0$  in this case. Since  $T_\phi = 100$  GeV, below this scale efficient leptogenesis is not possible in the Case (b) region in this figure.

Fig. 13 shows the shape of the sensitive regions for  $M_\phi = 10^5$  GeV and  $T_\phi = 100$  GeV assuming  $n_T = 0$ . We see that even for  $n_T = 0$ , UDECIGO, DECIGO, BBO,  $\mu$ -ARES can probe leptogenesis with  $T_\phi = 100$  GeV, given small mass  $M_\phi$  of the scalar. A small scalar mass injects less amount of entropy when they decay as a result of which the suppression is small, hence SNR is larger.

In Fig. 14 and 15 we show the SNR contours in the Case (c) region of two-step entropy injection assuming a non-vanishing coupling  $y_R$ . We make sure that the thermalization condition (B7) is satisfied for given parameter choices as well as the condition for two-stages of entropy injection,  $T_\phi > T_{\text{dom}}^{N_1}$  described in Sec. IV. In Fig. 14 we chose  $M_\phi = 10^{15}$  GeV,  $T_\phi = 10^{10}$  GeV and  $T_{\text{RH}} = 10^{16}$  GeV and demonstrate the effect of the spectral index  $n_T = 0$  (**Left**) and  $n_T = 0.5$  (**Right**). Note that instantaneous RHN decay scenario (Case (a)) is still possible in thermal scenario, denoted by the green shaded region. Fig. 15 is the same as Fig. 14 but for  $T_\phi = 10^6$  GeV.

We calculate the SNR contours for all these GW experiments taking various values of  $M_\phi$  and  $T_\phi$  for  $n_T = 0$  and 0.5, which we do not show in this paper. However, based on these results and Fig. 10-15, in Tables II and III, we summarize which key GW experiments can probe the parameter space  $M_1$  vs  $K$ , associated to thermal and non-thermal leptogenesis in the future with threshold  $\text{SNR} \geq 10$ , for these parameter choices. We see that thermal leptogenesis is possible only for high scalar mass  $M_\phi \sim 10^{15}$  GeV which U-DECIGO, BBO and  $\mu$ -ARES will be able to probe even for  $n_T = 0$  while LISA and ET requires  $n_T \gtrsim 0.5$ .

### C. Compatibility with NANOGrav

Several papers [48, 187–189] discuss the possibility of inflationary gravitational waves to be the source of the stochastic background detected in the recent NANOGrav data [47]. The NANOGrav collaboration [48] states the best fit is found to be around  $n_T \sim 2.61 \pm 0.85$ ,

$M_\phi$ (GeV)	$T_\phi$ (GeV)	U-DECIGO	BBO	$\mu$ -ARES	LISA	ET	CE
10 <sup>15</sup>	10 <sup>10</sup>	Non-Th, Th	Non-Th, Th	Non-Th, Th	-	-	Non-Th, Th
	10 <sup>6</sup>	Non-Th, Th	Non-Th, Th	Non-Th, Th	-	-	-
	10 <sup>2</sup>	-	-	-	-	-	-
10 <sup>10</sup>	10 <sup>6</sup>	Non-Th	Non-Th	Non-Th	-	-	-
	10 <sup>2</sup>	-	-	-	-	-	-
10 <sup>5</sup>	10 <sup>2</sup>	Non-Th	Non-Th	Non-Th	-	-	-

TABLE II: *Future sensitivity of different key experiments to probe the RHN parameter space ( $M_1$  vs.  $K$ ) with threshold SNR > 10, given benchmark values of  $M_\phi$  and  $T_\phi$  for  $n_T = 0$ . Non-Th and Th implies sensitivity of the specific experiment to non-thermal and thermal leptogenesis. Note that thermal scenario requires Eq. (B7) to be satisfied. Here we considered  $T_{\text{RH}} = 10^{16}$  GeV and maximal tensor-to-scalar ratio  $r = 0.035$ .*

$M_\phi$ (GeV)	$T_\phi$ (GeV)	U-DECIGO	BBO	$\mu$ -ARES	LISA	ET	CE
10 <sup>15</sup>	10 <sup>10</sup>	Non-Th, Th	Non-Th, Th	Non-Th, Th	Non-Th, Th	Non-Th, Th	Non-Th, Th
	10 <sup>6</sup>	Non-Th, Th	Non-Th, Th	Non-Th, Th	Non-Th, Th	Non-Th, Th	Non-Th, Th
	10 <sup>2</sup>	Non-Th	Non-Th	Non-Th	-	-	-
10 <sup>10</sup>	10 <sup>6</sup>	Non-Th	Non-Th	Non-Th	Non-Th	Non-Th	Non-Th
	10 <sup>2</sup>	Non-Th	Non-Th	Non-Th	Non-Th	Non-Th	Non-Th
10 <sup>5</sup>	10 <sup>2</sup>	Non-Th	Non-Th	Non-Th	Non-Th	Non-Th	Non-Th

TABLE III: *Same as Table. II but for  $n_T = 0.5$ . We see that most of the parameter space  $M_\phi$  vs  $T_\phi$  will be probed by future GW experiments if  $n_T = 0.5$ .*

$r \sim 10^{-14.06 \pm 5.82}$  and  $T_{\text{RH}} \sim 1$  GeV. However at such low reheating temperatures, efficient leptogenesis as we discussed in the paper is not possible due to sphaleron constraints.

## VII. DISCUSSION & CONCLUSION

Leptogenesis at low and intermediate energy scales provides an attractive scenario for baryogenesis, linking the observed the matter-antimatter asymmetry to the neutrino sector and seesaw scale. In this analysis, we offer a probe of this scenario via observations of the stochastic GW background that originates during inflation (which is responsible for the creation of primordial density perturbation of the Universe) and propagates in the post-inflationary era to reach us at the present time. Particularly we showed that detecting a characteristic GW spectral shape will represent a smoking gun for a RHN or

$\phi$  matter-dominated era in the early Universe. We present a minimal model realization of non-thermal leptogenesis, for which we found that a large fraction of the viable parameter space will be probed in future GW experiments. For the lightest RHN mass  $M_1$  and washout parameter  $K$  involving light-heavy neutrino Yukawa couplings  $\lambda$ , we find that  $M_1$  in the range  $100 \text{ GeV} \lesssim M_1 \lesssim 10^{14} \text{ GeV}$  and  $K$  for extremely weak washout ( $K \sim 10^{-20}$ ) and for strong washout ( $K \sim 10^4$ ) regime consistent with successful baryogenesis, novel GW shapes will be probes by U-DECIGO, DECIGO, BBO,  $\mu$ -ARES, LISA, CE, ET etc. By estimating signal-to-noise ratio (SNR) for GW experiments, we investigated the effect of the scalar mass  $M_\phi$  and decay temperature  $T_\phi$  which depends on the  $\phi$ - $N$  Yukawa couplings  $y_N$ .

The key interpretations of our results are summarized below:

- The overall SNR is larger for a larger spectral index  $n_T$  (compare for example Fig. 10 **Left** and **Right** plots).
- For vanishing Yukawa coupling  $y_R$  defined in the Lagrangian (19), we obtain non-thermal leptogenesis which can be probed in future GW experiments such as U-DECIGO, BBO etc. (see spectra in Fig. 5, 7 and SNR in Fig. 10, 11, 12, 13).
- Thermal leptogenesis with two-step entropy injection is possible with a non-zero  $y_R$  (Eq. (B6) and Fig. 14, 15). We propose the two-step entropy injection transfer function via Eq. (57) (see spectra in Fig. 8 and 9). Such two step will be detected in U-DECIGO, BBO,  $\mu$ -ARES etc. for  $n_T = 0$  and LISA, ET and CE as well for  $n_T = 0.5$ .
- If  $T_{N_1} < T_\phi$ , then lower values of  $M_1$  and  $K$  reduce SNR and therefore challenging to test for all experiments (Fig. 10, 11, 12, 13, 14, 15).
- If  $T_\phi < T_{N_1}$  in the non-thermal scenario, a lower  $T_\phi$  value decreases the SNR and frequency of suppression  $f_{\text{sup}}$  given in Eq. (55), making it more difficult to observe (see spectra in Fig. 5,6). However, suitable low values of  $T_\phi$  increases the overall GW sensitive region in the parameter space of the lightest RHN (compare Case (a) regions in Fig. 10, 11 and 12). The Case (a) scenario is discussed in Sec. IV.
- A higher  $M_\phi$  means larger entropy injection which decreases the overall SNR values for all experiments (see spectra in Fig. 5, 6, 7, 9).  $M_\phi$  also sets the upper bound on

$M_1$  in our model, i.e.  $M_1 \leq M_\phi/2$ . We are interested in the parameter space where  $\phi$  is long lived in order to dominate the energy Budget of the Universe (see discussion following Eq. (25) and Eq. (29)).

- In Case (a) described in Sec. IV, where RHNs decay instantaneously after production from  $\phi$  decay, the leptogenesis scale is  $\sim T_\phi$  which means GW experiments can probe leptogenesis even for strong washout  $K > 1$  where RHNs do not dominate the energy budget of the Universe (Fig. 10, 11, 12, 13). This is unlike thermal leptogenesis [61] where the RHN domination criterion  $K \lesssim 10^{-4}$  given in Eq. (33) must be satisfied for GW sensitivity.
- Table II and III summarize which key experiments can probe thermal and non-thermal leptogenesis for  $n_T = 0$  and 0.5 respectively, given benchmark values of the scalar mass  $M_\phi$  and scalar decay temperature  $T_\phi$ .

If the characteristic features of the GW spectral shapes proposed in this study are observed one may look to target additional observations in order to distinguish between a RHN or scalar  $\phi$  dominated pre-BBN era and other forms of early matter domination. Particularly in low-scale leptogenesis RHN masses of GeV-TeV could be searched in typical Heavy Neutral Lepton Searches (HNL) search experiments (see [190–192] for current experimental limits) at the particle physics laboratories. In this manner we can complement GW searches with laboratory searches in the same BSM parameter space. however such a study is beyond the reach of the present paper and we plan to explore this in future. RH neutrinos, if they exist should also show up in experiments such as neutrino-less double beta decay [193, 194] or lepton number violating processes [195, 196] and therefore provide us with a myriad of pathways to independently verify the existence of an early RHN-domination or scalar domination era. This leads to a unique and exciting opportunity to form synergies between GW searches and laboratory and CMB searches.

### Acknowledgments

ZAB is supported by a DST-INSPIRE fellowship. LM is supported by a UGC fellowship. Authors thank Prof. Kai Schmidt for his valuable comments on the NANOGrav best fit.

## Appendix A: Change of Variable

It is convenient to use comoving variables while solving the Boltzmann equations. We adopt the same prescription as in [99, 197],

$$E_{\phi, N_i} = \rho_{\phi, N_i} a^3, \quad \tilde{N}_i = n_i a^3 = \frac{\rho_{N_i}}{M_i} a^3, \quad \tilde{N}_{\text{B-L}} = n_{\text{B-L}} a^3, \quad R = \rho_R a^4, \quad S = s a^3 \quad (\text{A1})$$

where  $a$  is the scale factor of the Universe. Instead of time  $t$ , we write the Boltzmann equations in terms of the ratio of scale factor  $a$  to its initial value  $a_I$ , given by,

$$y = \frac{a}{a_I} \quad (\text{A2})$$

We take  $a_I = 1$  without loss of generality. The expansion rate can be written as,

$$H = \sqrt{\frac{8\pi(a_I E_\phi y + a_I E_{N_1} y + a_I E_{N_2} y + R)}{3M_{\text{pl}}^2 a_I^4 y^4}} \quad (\text{A3})$$

The temperature can be written as,

$$T = \left[ \frac{30 R}{\pi^2 g_* a_I^4 y^4} \right]^{\frac{1}{4}} \quad (\text{A4})$$

However this is not the actual temperature of the Universe during the early matter dominated epoch. The maximum possible temperature can be approximated as,

$$T_{\text{tot}} = \left[ \frac{30 (R + E_\phi + E_{N_1} + E_{N_2})}{\pi^2 g_* a_I^4 y^4} \right]^{\frac{1}{4}} \quad (\text{A5})$$

The redshift parameter  $z$  is defined in terms of  $M_1$ ,

$$z = \frac{M_1}{T} = M_1 a_I \left[ \frac{\pi^2 g_*}{30 R} \right]^{\frac{1}{4}} y \quad (\text{A6})$$

The equilibrium energy densities are given by [99, 198],

$$\begin{aligned} E_{N_i}^{eq} &= \rho_{N_i}^{eq} a^3 = \frac{a_I^3 M_i^4 y^3}{\pi^2} \left[ \frac{3}{z^2} K_2(z) + \frac{1}{z} K_1(z) \right], & \tilde{N}_i^{eq} &= \frac{E_{N_i}^{eq}}{M_i}, \\ n_{N_i}^{eq} &= \frac{E_{N_i}^{eq}}{M_i y^3}, & n_R^{eq} &= \frac{3\zeta(3)}{4\pi^2} \times 2 \left( \frac{M_1}{z(y)} \right)^3 \end{aligned} \quad (\text{A7})$$

The inverse decay rate can be written as [105],

$$\Gamma_{ID} = \frac{1}{2} \sum_{i=1}^2 \Gamma_{N_i} \frac{n_{N_i}^{eq}}{n_R^{eq}} \quad (\text{A8})$$

Now we can write the Boltzmann equations given in Eq. (30) in terms of the comoving energy densities as,

$$\begin{aligned}
\frac{dE_\phi}{dy} &= -\frac{\Gamma_\phi E_\phi}{\mathcal{H} y}, \\
\frac{dE_{N_1}}{dy} &= \frac{\Gamma_{\phi \rightarrow N_1 N_1} E_\phi}{\mathcal{H} y} - \frac{\Gamma_{N_1}}{\mathcal{H} y} (E_{N_1} - E_{N_1}^{eq}), \\
\frac{dE_{N_2}}{dy} &= \frac{\Gamma_{\phi \rightarrow N_2 N_2} E_\phi}{\mathcal{H} y} - \frac{\Gamma_{N_2}}{\mathcal{H} y} (E_{N_2} - E_{N_2}^{eq}), \\
\frac{d\tilde{N}_{B-L}}{dy} &= -\sum_{i=1}^2 \frac{\Gamma_{N_i}}{\mathcal{H} y} \left[ \epsilon (\tilde{N}_i - \tilde{N}_i^{eq}) + \frac{1}{2} \frac{n_{N_i}^{eq}}{n_R^{eq}} \tilde{N}_{B-L} \right], \\
\frac{dR}{dy} &= \frac{\Gamma_{\phi \rightarrow R} E_\phi}{\mathcal{H}} + \sum_{i=1}^2 \frac{\Gamma_{N_i}}{\mathcal{H}} (E_{N_i} - E_{N_i}^{eq})
\end{aligned} \tag{A9}$$

By solving the above equations, one can calculate the efficiency parameter to be,

$$\kappa_f = -\frac{4}{3} \epsilon^{-1} R^{-3/4} \tilde{N}_{B-L} \left[ \frac{\pi^4 g_*^{3/4}}{30^3 \zeta(3)^4} \right] \tag{A10}$$

## Appendix B: Thermalization of RHNs

For extremely weak washout  $K \ll 1$ , i.e. small light-heavy Yukawa couplings  $\lambda$ , RHNs can never attain thermal equilibrium with the radiation bath via decay and inverse decay. Here we show that in presence of a non-vanishing coupling  $y_R$  with radiation, they can be thermalized through the 2-to-2 scattering process  $N_i N_i \leftrightarrow \bar{f} f$  via  $\phi$ . We are interested in thermalization of  $N_1$  during the  $\phi$ -dominated epoch. The necessary condition is,

$$\Gamma_{\text{SC}} \gtrsim \mathcal{H}(T) \tag{B1}$$

where  $\Gamma_{\text{SC}}$  is the scattering width of the 2-to-2 scattering process and  $\mathcal{H}(T) \sim \frac{T^4}{M_{\text{pl}} T_\phi^2}$  is the Hubble parameter at temperature  $T$  during the  $\phi$ -dominated epoch [199, 200]. The scattering rate can be approximated from the scattering cross section  $\sigma_c$  [130],

$$\Gamma_{\text{SC}} = \sigma_c |v_{\text{rel}}| n^{\text{eq}} \tag{B2}$$

where  $v_{\text{rel}}$  is the relative velocity between the projectile and target particles and  $n^{\text{eq}}$  is the equilibrium number density of RHNs. Here we assumed that the cross section is velocity independent. During  $\phi$  dominated era,  $T \gg m_f$  where  $m_f$  is the mass of the fermion. Hence fermions are relativistic with energy  $\sim T$ . We also assume the RHNs produced from  $\phi$

are relativistic as well. Since  $\phi$  is non-thermal, its temperature need not be same as the radiation temperature, nevertheless we approximate it to be  $\mathcal{O}(T)$ , such that  $|v_{\text{rel}}| = c = 1$  and  $n^{\text{eq}} \sim T^3$  [201]. The total cross-section in the center-of-mass frame of the scalar is given by,

$$\sigma_c \sim \int \frac{|\overline{\mathcal{M}}|^2}{(E_1 + E_2)^2} d\Omega \quad (\text{B3})$$

where  $E_1 \sim E_2 \sim T$  are the energies of the incident particles and  $\mathcal{M}$  is the Feynmann amplitude with over-line implying average over spin or polarization states. The integral is performed over solid angle  $\Omega$ . We have considered the magnitude of the 3-momenta of the incoming and outgoing particles to be equal. At tree level we get,

$$|\overline{\mathcal{M}}|^2 \sim (y_R y_{N_1})^2 \quad (\text{B4})$$

Then the scattering rate is given by,

$$\Gamma_{\text{SC}} \sim (y_R y_{N_1})^2 T \quad (\text{B5})$$

Therefore Eq. B1 becomes,

$$y_R y_{N_1} \gtrsim \sqrt{\frac{T^3}{M_{\text{pl}} T_\phi^2}} \quad (\text{B6})$$

Taking  $T = T_\phi$  in the above equation, one obtains the approximate condition for the RHNs to be in thermal equilibrium till  $T_\phi$ . Then at a lower temperature, the RHNs decouples and freezes out until their decay. For example, for RHNs to freeze out at around  $T_\phi \sim 10^5$  GeV we need  $y_R y_{N_1} \sim 10^{-7}$ .

The two-step entropy injection scenario is possible when Eq. (B6) along with the condition for  $\phi$  domination given in (29) are satisfied simultaneously. Solving both of them simultaneously, we obtain the condition on scalar mass for the two-step entropy injection scenario,

$$M_\phi \gtrsim 2\sqrt{T_\phi M_{\text{pl}}} + M_{\text{pl}} (y_{N_1} - y_R)^2 \gtrsim 2\sqrt{T_\phi M_{\text{pl}}} \quad (\text{B7})$$

where the last inequality is the minimum requirement for  $M_\phi$  for which thermal scenario is possible when  $y_{N_1} \sim y_R$ .

- 
- [1] SUPER-KAMIOKANDE collaboration, *Constraints on neutrino oscillations using 1258 days of Super-Kamiokande solar neutrino data*, *Phys. Rev. Lett.* **86** (2001) 5656 [hep-ex/0103033].
- [2] SUPER-KAMIOKANDE collaboration, *Determination of solar neutrino oscillation parameters using 1496 days of Super-Kamiokande I data*, *Phys. Lett. B* **539** (2002) 179 [hep-ex/0205075].
- [3] SNO collaboration, *Direct evidence for neutrino flavor transformation from neutral current interactions in the Sudbury Neutrino Observatory*, *Phys. Rev. Lett.* **89** (2002) 011301 [nucl-ex/0204008].
- [4] SUPER-KAMIOKANDE collaboration, *A Measurement of atmospheric neutrino oscillation parameters by SUPER-KAMIOKANDE I*, *Phys. Rev. D* **71** (2005) 112005 [hep-ex/0501064].
- [5] SUPER-KAMIOKANDE collaboration, *Solar Neutrino Measurements in Super-Kamiokande-IV*, *Phys. Rev. D* **94** (2016) 052010 [1606.07538].
- [6] BOREXINO collaboration, *Measurement of neutrino flux from the primary proton–proton fusion process in the Sun with Borexino detector*, *Phys. Part. Nucl.* **47** (2016) 995 [1507.02432].
- [7] ICECUBE collaboration, *Measurement of Atmospheric Neutrino Oscillations at 6–56 GeV with IceCube DeepCore*, *Phys. Rev. Lett.* **120** (2018) 071801 [1707.07081].
- [8] ANTARES collaboration, *Measuring the atmospheric neutrino oscillation parameters and constraining the 3+1 neutrino model with ten years of ANTARES data*, *JHEP* **06** (2019) 113 [1812.08650].
- [9] KAMLAND collaboration, *Precision Measurement of Neutrino Oscillation Parameters with KamLAND*, *Phys. Rev. Lett.* **100** (2008) 221803 [0801.4589].
- [10] T2K collaboration, *Indication of Electron Neutrino Appearance from an Accelerator-produced Off-axis Muon Neutrino Beam*, *Phys. Rev. Lett.* **107** (2011) 041801 [1106.2822].
- [11] DOUBLE CHOOZ collaboration, *Indication of Reactor  $\bar{\nu}_e$  Disappearance in the Double Chooz Experiment*, *Phys. Rev. Lett.* **108** (2012) 131801 [1112.6353].
- [12] T2K collaboration, *Observation of Electron Neutrino Appearance in a Muon Neutrino*

- Beam*, *Phys. Rev. Lett.* **112** (2014) 061802 [1311.4750].
- [13] KATRIN collaboration, *Direct neutrino-mass measurement with sub-electronvolt sensitivity*, *Nature Phys.* **18** (2022) 160 [2105.08533].
- [14] PLANCK collaboration, *Planck 2018 results. VI. Cosmological parameters*, *Astron. Astrophys.* **641** (2020) A6 [1807.06209].
- [15] PLANCK collaboration, *Planck 2018 results. VI. Cosmological parameters*, *Astron. Astrophys.* **641** (2020) A6 [1807.06209].
- [16] EBOSS collaboration, *Completed SDSS-IV extended Baryon Oscillation Spectroscopic Survey: Cosmological implications from two decades of spectroscopic surveys at the Apache Point Observatory*, *Phys. Rev. D* **103** (2021) 083533 [2007.08991].
- [17] PARTICLE DATA GROUP collaboration, *Review of Particle Physics*, *PTEP* **2020** (2020) 083C01.
- [18] B.D. Fields, K.A. Olive, T.-H. Yeh and C. Young, *Big-Bang Nucleosynthesis after Planck*, *JCAP* **03** (2020) 010 [1912.01132].
- [19] P. Minkowski,  $\mu \rightarrow e\gamma$  at a Rate of One Out of  $10^9$  Muon Decays?, *Phys. Lett. B* **67** (1977) 421.
- [20] T. Yanagida, *Horizontal gauge symmetry and masses of neutrinos*, *Conf. Proc. C* **7902131** (1979) 95.
- [21] S.L. Glashow, *The Future of Elementary Particle Physics*, *NATO Sci. Ser. B* **61** (1980) 687.
- [22] R.N. Mohapatra and G. Senjanovic, *Neutrino Mass and Spontaneous Parity Nonconservation*, *Phys. Rev. Lett.* **44** (1980) 912.
- [23] M. Fukugita and T. Yanagida, *Baryogenesis Without Grand Unification*, *Phys. Lett. B* **174** (1986) 45.
- [24] E. Nardi, Y. Nir, E. Roulet and J. Racker, *The Importance of flavor in leptogenesis*, *JHEP* **01** (2006) 164 [hep-ph/0601084].
- [25] A. Abada, S. Davidson, F.-X. Josse-Michaux, M. Losada and A. Riotto, *Flavor issues in leptogenesis*, *JCAP* **04** (2006) 004 [hep-ph/0601083].
- [26] A. Abada, S. Davidson, A. Ibarra, F.X. Josse-Michaux, M. Losada and A. Riotto, *Flavour Matters in Leptogenesis*, *JHEP* **09** (2006) 010 [hep-ph/0605281].
- [27] S. Davidson and A. Ibarra, *A Lower bound on the right-handed neutrino mass from leptogenesis*, *Phys. Lett. B* **535** (2002) 25 [hep-ph/0202239].

- [28] G.F. Giudice, A. Notari, M. Raidal, A. Riotto and A. Strumia, *Towards a complete theory of thermal leptogenesis in the SM and MSSM*, *Nucl. Phys. B* **685** (2004) 89 [hep-ph/0310123].
- [29] V. Cirigliano et al., *Neutrinoless Double-Beta Decay: A Roadmap for Matching Theory to Experiment*, 2203.12169.
- [30] T. Endoh, S. Kaneko, S.K. Kang, T. Morozumi and M. Tanimoto, *CP violation in neutrino oscillation and leptogenesis*, *Phys. Rev. Lett.* **89** (2002) 231601 [hep-ph/0209020].
- [31] P. Di Bari and A. Riotto, *Successful type I Leptogenesis with  $SO(10)$ -inspired mass relations*, *Phys. Lett. B* **671** (2009) 462 [0809.2285].
- [32] E. Bertuzzo, P. Di Bari and L. Marzola, *The problem of the initial conditions in flavoured leptogenesis and the tauon  $N_2$ -dominated scenario*, *Nucl. Phys. B* **849** (2011) 521 [1007.1641].
- [33] F. Buccella, D. Falcone, C.S. Fong, E. Nardi and G. Ricciardi, *Squeezing out predictions with leptogenesis from  $SO(10)$* , *Phys. Rev. D* **86** (2012) 035012 [1203.0829].
- [34] G. Altarelli and D. Meloni, *A non supersymmetric  $SO(10)$  grand unified model for all the physics below  $M_{GUT}$* , *JHEP* **08** (2013) 021 [1305.1001].
- [35] C.S. Fong, D. Meloni, A. Meroni and E. Nardi, *Leptogenesis in  $SO(10)$* , *JHEP* **01** (2015) 111 [1412.4776].
- [36] V.S. Mummidi and K.M. Patel, *Leptogenesis and fermion mass fit in a renormalizable  $SO(10)$  model*, *JHEP* **12** (2021) 042 [2109.04050].
- [37] K.M. Patel, *Minimal spontaneous CP-violating GUT and predictions for leptonic CP phases*, *Phys. Rev. D* **107** (2023) 075041 [2212.04095].
- [38] S. Ipek, A.D. Plascencia and J. Turner, *Assessing Perturbativity and Vacuum Stability in High-Scale Leptogenesis*, *JHEP* **12** (2018) 111 [1806.00460].
- [39] D. Croon, N. Fernandez, D. McKeen and G. White, *Stability, reheating and leptogenesis*, *JHEP* **06** (2019) 098 [1903.08658].
- [40] LIGO SCIENTIFIC, VIRGO collaboration, *Observation of Gravitational Waves from a Binary Black Hole Merger*, *Phys. Rev. Lett.* **116** (2016) 061102 [1602.03837].
- [41] LIGO SCIENTIFIC, VIRGO collaboration, *GW151226: Observation of Gravitational Waves from a 22-Solar-Mass Binary Black Hole Coalescence*, *Phys. Rev. Lett.* **116** (2016) 241103 [1606.04855].

- [42] C.L. Carilli and S. Rawlings, *Science with the Square Kilometer Array: Motivation, key science projects, standards and assumptions*, *New Astron. Rev.* **48** (2004) 979 [astro-ph/0409274].
- [43] G. Janssen et al., *Gravitational wave astronomy with the SKA*, *PoS AASKA14* (2015) 037 [1501.00127].
- [44] A. Weltman et al., *Fundamental physics with the Square Kilometre Array*, *Publ. Astron. Soc. Austral.* **37** (2020) e002 [1810.02680].
- [45] EPTA collaboration, *European Pulsar Timing Array Limits On An Isotropic Stochastic Gravitational-Wave Background*, *Mon. Not. Roy. Astron. Soc.* **453** (2015) 2576 [1504.03692].
- [46] EPTA collaboration, *European Pulsar Timing Array Limits on Continuous Gravitational Waves from Individual Supermassive Black Hole Binaries*, *Mon. Not. Roy. Astron. Soc.* **455** (2016) 1665 [1509.02165].
- [47] NANOGrav collaboration, *The NANOGrav 15 yr Data Set: Evidence for a Gravitational-wave Background*, *Astrophys. J. Lett.* **951** (2023) L8 [2306.16213].
- [48] NANOGrav collaboration, *The NANOGrav 15 yr Data Set: Search for Signals from New Physics*, *Astrophys. J. Lett.* **951** (2023) L11 [2306.16219].
- [49] A. Ghoshal, D. Nanda and A.K. Saha, *CMB imprints of high scale non-thermal leptogenesis*, *Phys. Lett. B* **849** (2024) 138484 [2210.14176].
- [50] J.A. Dror, T. Hiramatsu, K. Kohri, H. Murayama and G. White, *Testing the Seesaw Mechanism and Leptogenesis with Gravitational Waves*, *Phys. Rev. Lett.* **124** (2020) 041804 [1908.03227].
- [51] S. Saad, *Probing minimal grand unification through gravitational waves, proton decay, and fermion masses*, *JHEP* **04** (2023) 058 [2212.05291].
- [52] P. Di Bari, S.F. King and M.H. Rahat, *Gravitational waves from phase transitions and cosmic strings in neutrino mass models with multiple Majorons*, 2306.04680.
- [53] S. Blasi, V. Brdar and K. Schmitz, *Fingerprint of low-scale leptogenesis in the primordial gravitational-wave spectrum*, *Phys. Rev. Res.* **2** (2020) 043321 [2004.02889].
- [54] B. Fu, A. Ghoshal and S.F. King, *Cosmic string gravitational waves from global  $U(1)_{B-L}$  symmetry breaking as a probe of the type I seesaw scale*, *JHEP* **11** (2023) 071 [2306.07334].
- [55] B. Barman, D. Borah, A. Dasgupta and A. Ghoshal, *Probing high scale Dirac leptogenesis*

- via gravitational waves from domain walls, Phys. Rev. D* **106** (2022) 015007 [2205.03422].
- [56] S.F. King, D. Marfatia and M.H. Rahat, *Towards distinguishing Dirac from Majorana neutrino mass with gravitational waves*, 2306.05389.
- [57] A. Dasgupta, P.S.B. Dev, A. Ghoshal and A. Mazumdar, *Gravitational wave pathway to testable leptogenesis*, *Phys. Rev. D* **106** (2022) 075027 [2206.07032].
- [58] D. Borah, A. Dasgupta and I. Saha, *Leptogenesis and dark matter through relativistic bubble walls with observable gravitational waves*, *JHEP* **11** (2022) 136 [2207.14226].
- [59] D.I. Dunsky, A. Ghoshal, H. Murayama, Y. Sakahihara and G. White, *GUTs, hybrid topological defects, and gravitational waves*, *Phys. Rev. D* **106** (2022) 075030 [2111.08750].
- [60] A. Ghoshal, R. Samanta and G. White, *Bremsstrahlung high-frequency gravitational wave signatures of high-scale nonthermal leptogenesis*, *Phys. Rev. D* **108** (2023) 035019 [2211.10433].
- [61] M. Berbig and A. Ghoshal, *Impact of high-scale Seesaw and Leptogenesis on inflationary tensor perturbations as detectable gravitational waves*, *JHEP* **05** (2023) 172 [2301.05672].
- [62] Z.A. Borboruah, A. Ghoshal and S. Ipek, *Probing flavor violation and baryogenesis via primordial gravitational waves*, 2405.03241.
- [63] Y.F. Perez-Gonzalez and J. Turner, *Assessing the tension between a black hole dominated early universe and leptogenesis*, *Phys. Rev. D* **104** (2021) 103021 [2010.03565].
- [64] S. Datta, A. Ghosal and R. Samanta, *Baryogenesis from ultralight primordial black holes and strong gravitational waves from cosmic strings*, *JCAP* **08** (2021) 021 [2012.14981].
- [65] S. Jyoti Das, D. Mahanta and D. Borah, *Low scale leptogenesis and dark matter in the presence of primordial black holes*, *JCAP* **11** (2021) 019 [2104.14496].
- [66] B. Barman, D. Borah, S.J. Das and R. Roshan, *Non-thermal origin of asymmetric dark matter from inflaton and primordial black holes*, *JCAP* **03** (2022) 031 [2111.08034].
- [67] N. Bernal, C.S. Fong, Y.F. Perez-Gonzalez and J. Turner, *Rescuing high-scale leptogenesis using primordial black holes*, *Phys. Rev. D* **106** (2022) 035019 [2203.08823].
- [68] N. Bhaumik, A. Ghoshal and M. Lewicki, *Doubly peaked induced stochastic gravitational wave background: testing baryogenesis from primordial black holes*, *JHEP* **07** (2022) 130 [2205.06260].
- [69] N. Bhaumik, A. Ghoshal, R.K. Jain and M. Lewicki, *Distinct signatures of spinning PBH domination and evaporation: doubly peaked gravitational waves, dark relics and CMB*

- complementarity*, *JHEP* **05** (2023) 169 [2212.00775].
- [70] A. Ghoshal, Y.F. Perez-Gonzalez and J. Turner, *Superradiant leptogenesis*, *JHEP* **02** (2024) 113 [2312.06768].
- [71] Y. Cui and Z.-Z. Xianyu, *Probing Leptogenesis with the Cosmological Collider*, *Phys. Rev. Lett.* **129** (2022) 111301 [2112.10793].
- [72] C.S. Fong, A. Ghoshal, A. Naskar, M.H. Rahat and S. Saad, *Primordial non-Gaussianity as a probe of seesaw and leptogenesis*, *JHEP* **11** (2023) 182 [2307.07550].
- [73] L.P. Grishchuk, *Amplification of gravitational waves in an isotropic universe*, *Zh. Eksp. Teor. Fiz.* **67** (1974) 825.
- [74] A.A. Starobinsky, *Spectrum of relict gravitational radiation and the early state of the universe*, *JETP Lett.* **30** (1979) 682.
- [75] V.A. Rubakov, M.V. Sazhin and A.V. Veryaskin, *Graviton Creation in the Inflationary Universe and the Grand Unification Scale*, *Phys. Lett. B* **115** (1982) 189.
- [76] M.C. Guzzetti, N. Bartolo, M. Liguori and S. Matarrese, *Gravitational waves from inflation*, *Riv. Nuovo Cim.* **39** (2016) 399 [1605.01615].
- [77] N. Seto and J. Yokoyama, *Probing the equation of state of the early universe with a space laser interferometer*, *J. Phys. Soc. Jap.* **72** (2003) 3082 [gr-qc/0305096].
- [78] L.A. Boyle and P.J. Steinhardt, *Probing the early universe with inflationary gravitational waves*, *Phys. Rev. D* **77** (2008) 063504 [astro-ph/0512014].
- [79] L.A. Boyle and A. Buonanno, *Relating gravitational wave constraints from primordial nucleosynthesis, pulsar timing, laser interferometers, and the CMB: Implications for the early Universe*, *Phys. Rev. D* **78** (2008) 043531 [0708.2279].
- [80] S. Kuroyanagi, T. Chiba and N. Sugiyama, *Precision calculations of the gravitational wave background spectrum from inflation*, *Phys. Rev. D* **79** (2009) 103501 [0804.3249].
- [81] K. Nakayama and J. Yokoyama, *Gravitational Wave Background and Non-Gaussianity as a Probe of the Curvaton Scenario*, *JCAP* **01** (2010) 010 [0910.0715].
- [82] S. Kuroyanagi, C. Ringeval and T. Takahashi, *Early universe tomography with CMB and gravitational waves*, *Phys. Rev. D* **87** (2013) 083502 [1301.1778].
- [83] R. Jinno, T. Moroi and K. Nakayama, *Inflationary Gravitational Waves and the Evolution of the Early Universe*, *JCAP* **01** (2014) 040 [1307.3010].
- [84] K. Saikawa and S. Shirai, *Primordial gravitational waves, precisely: The role of*

- thermodynamics in the Standard Model*, *JCAP* **05** (2018) 035 [1803.01038].
- [85] C. Chen, K. Dimopoulos, C. Eröncel and A. Ghoshal, *Enhanced primordial gravitational waves from a stiff post-inflationary era due to an oscillating inflaton*, 2405.01679.
- [86] N. Bernal, A. Ghoshal, F. Hajkarim and G. Lambiase, *Primordial Gravitational Wave Signals in Modified Cosmologies*, *JCAP* **11** (2020) 051 [2008.04959].
- [87] K. Nakayama, S. Saito, Y. Suwa and J. Yokoyama, *Space laser interferometers can determine the thermal history of the early Universe*, *Phys. Rev. D* **77** (2008) 124001 [0802.2452].
- [88] K. Nakayama, S. Saito, Y. Suwa and J. Yokoyama, *Probing reheating temperature of the universe with gravitational wave background*, *JCAP* **06** (2008) 020 [0804.1827].
- [89] S. Kuroyanagi, K. Nakayama and S. Saito, *Prospects for determination of thermal history after inflation with future gravitational wave detectors*, *Phys. Rev. D* **84** (2011) 123513 [1110.4169].
- [90] W. Buchmüller, V. Domcke, K. Kamada and K. Schmitz, *The Gravitational Wave Spectrum from Cosmological  $B - L$  Breaking*, *JCAP* **10** (2013) 003 [1305.3392].
- [91] W. Buchmüller, V. Domcke, K. Kamada and K. Schmitz, *A Minimal Supersymmetric Model of Particle Physics and the Early Universe*, 1309.7788.
- [92] R. Jinno, T. Moroi and T. Takahashi, *Studying Inflation with Future Space-Based Gravitational Wave Detectors*, *JCAP* **12** (2014) 006 [1406.1666].
- [93] S. Kuroyanagi, K. Nakayama and J. Yokoyama, *Prospects of determination of reheating temperature after inflation by DECIGO*, *PTEP* **2015** (2015) 013E02 [1410.6618].
- [94] A. Ghoshal, Y. Gouttenoire, L. Heurtier and P. Simakachorn, *Primordial black hole archaeology with gravitational waves from cosmic strings*, *JHEP* **08** (2023) 196 [2304.04793].
- [95] A. Ghoshal, L. Heurtier and A. Paul, *Signatures of non-thermal dark matter with kination and early matter domination. Gravitational waves versus laboratory searches*, *JHEP* **12** (2022) 105 [2208.01670].
- [96] R.J. Scherrer and M.S. Turner, *Decaying Particles Do Not Heat Up the Universe*, *Phys. Rev. D* **31** (1985) 681.
- [97] E.W. Kolb and M.S. Turner, *The Early Universe*, vol. 69 (1990), 10.1201/9780429492860.
- [98] F. Bezrukov, H. Hettmansperger and M. Lindner, *keV sterile neutrino Dark Matter in*

- gauge extensions of the Standard Model*, *Phys. Rev. D* **81** (2010) 085032 [0912.4415].
- [99] F. Hahn-Woernle and M. Plumacher, *Effects of reheating on leptogenesis*, *Nucl. Phys. B* **806** (2009) 68 [0801.3972].
- [100] X. Zhang, *Towards a systematic study of non-thermal leptogenesis from inflaton decays*, 2311.05824.
- [101] T. Yanagida, *Leptogenesis in the early universe*, *Phys. Scripta T* **121** (2005) 137.
- [102] J.A. Harvey and M.S. Turner, *Cosmological baryon and lepton number in the presence of electroweak fermion number violation*, *Phys. Rev. D* **42** (1990) 3344.
- [103] S.Y. Khlebnikov and M.E. Shaposhnikov, *The Statistical Theory of Anomalous Fermion Number Nonconservation*, *Nucl. Phys. B* **308** (1988) 885.
- [104] M.A. Luty, *Baryogenesis via leptogenesis*, *Phys. Rev. D* **45** (1992) 455.
- [105] W. Buchmuller, P. Di Bari and M. Plumacher, *Leptogenesis for pedestrians*, *Annals Phys.* **315** (2005) 305 [hep-ph/0401240].
- [106] P.B. Arnold and L.D. McLerran, *Sphalerons, Small Fluctuations and Baryon Number Violation in Electroweak Theory*, *Phys. Rev. D* **36** (1987) 581.
- [107] E. Nardi, J. Racker and E. Roulet, *CP violation in scatterings, three body processes and the Boltzmann equations for leptogenesis*, *JHEP* **09** (2007) 090 [0707.0378].
- [108] A. Basboll and S. Hannestad, *Decay of heavy Majorana neutrinos using the full Boltzmann equation including its implications for leptogenesis*, *JCAP* **01** (2007) 003 [hep-ph/0609025].
- [109] M. Flanz, E.A. Paschos and U. Sarkar, *Baryogenesis from a lepton asymmetric universe*, *Phys. Lett. B* **345** (1995) 248 [hep-ph/9411366].
- [110] L. Covi, E. Roulet and F. Vissani, *CP violating decays in leptogenesis scenarios*, *Phys. Lett. B* **384** (1996) 169 [hep-ph/9605319].
- [111] W. Buchmuller and M. Plumacher, *CP asymmetry in Majorana neutrino decays*, *Phys. Lett. B* **431** (1998) 354 [hep-ph/9710460].
- [112] W. Buchmuller, P. Di Bari and M. Plumacher, *The Neutrino mass window for baryogenesis*, *Nucl. Phys. B* **665** (2003) 445 [hep-ph/0302092].
- [113] W. Buchmuller, P. Di Bari and M. Plumacher, *Some aspects of thermal leptogenesis*, *New J. Phys.* **6** (2004) 105 [hep-ph/0406014].
- [114] T. Hambye, Y. Lin, A. Notari, M. Papucci and A. Strumia, *Constraints on neutrino masses from leptogenesis models*, *Nucl. Phys. B* **695** (2004) 169 [hep-ph/0312203].

- [115] W. Buchmuller, P. Di Bari and M. Plumacher, *Cosmic microwave background, matter - antimatter asymmetry and neutrino masses*, *Nucl. Phys. B* **643** (2002) 367 [hep-ph/0205349].
- [116] W. Buchmuller, R.D. Peccei and T. Yanagida, *Leptogenesis as the origin of matter*, *Ann. Rev. Nucl. Part. Sci.* **55** (2005) 311 [hep-ph/0502169].
- [117] F. Vissani, *Do experiments suggest a hierarchy problem?*, *Phys. Rev. D* **57** (1998) 7027 [hep-ph/9709409].
- [118] J.D. Clarke, R. Foot and R.R. Volkas, *Electroweak naturalness in the three-flavor type I seesaw model and implications for leptogenesis*, *Phys. Rev. D* **91** (2015) 073009 [1502.01352].
- [119] S. Datta and R. Samanta, *Gravitational waves-tomography of Low-Scale-Leptogenesis*, *JHEP* **11** (2022) 159 [2208.09949].
- [120] M. Drees and Y. Xu, *Small field polynomial inflation: reheating, radiative stability and lower bound*, *JCAP* **09** (2021) 012 [2104.03977].
- [121] A. Ghoshal, N. Okada and A. Paul, *eV Hubble scale inflation with a radiative plateau: Very light inflaton, reheating, and dark matter in B-L extensions*, *Phys. Rev. D* **106** (2022) 095021 [2203.03670].
- [122] M. Kawasaki, K. Kohri and T. Moroi, *Big-Bang nucleosynthesis and hadronic decay of long-lived massive particles*, *Phys. Rev. D* **71** (2005) 083502 [astro-ph/0408426].
- [123] A. Pilaftsis, *Resonant CP violation induced by particle mixing in transition amplitudes*, *Nucl. Phys. B* **504** (1997) 61 [hep-ph/9702393].
- [124] A. Pilaftsis, *CP violation and baryogenesis due to heavy Majorana neutrinos*, *Phys. Rev. D* **56** (1997) 5431 [hep-ph/9707235].
- [125] A. Pilaftsis and T.E.J. Underwood, *Electroweak-scale resonant leptogenesis*, *Phys. Rev. D* **72** (2005) 113001 [hep-ph/0506107].
- [126] J. Klarić, M. Shaposhnikov and I. Timiryasov, *Uniting Low-Scale Leptogenesis Mechanisms*, *Phys. Rev. Lett.* **127** (2021) 111802 [2008.13771].
- [127] T. Asaka, K. Hamaguchi, M. Kawasaki and T. Yanagida, *Leptogenesis in inflaton decay*, *Phys. Lett. B* **464** (1999) 12 [hep-ph/9906366].
- [128] M. Nemevšek and Y. Zhang, *Anatomy of Diluted Dark Matter in the Minimal Left-Right Symmetric Model*, 2312.00129.

- [129] A. Ghoshal, N. Okada and A. Paul, *Radiative plateau inflation with conformal invariance: Dynamical generation of electroweak and seesaw scales*, *Phys. Rev. D* **106** (2022) 055024 [2203.00677].
- [130] A. Ghoshal, Z. Lalak and S. Porey, *Measuring inflaton couplings via dark radiation as  $\Delta N_{\text{eff}}$  in CMB*, *Phys. Rev. D* **108** (2023) 063030 [2302.03268].
- [131] G.F. Giudice, M. Peloso, A. Riotto and I. Tkachev, *Production of massive fermions at preheating and leptogenesis*, *JHEP* **08** (1999) 014 [hep-ph/9905242].
- [132] PLANCK collaboration, *Planck 2018 results. X. Constraints on inflation*, *Astron. Astrophys.* **641** (2020) A10 [1807.06211].
- [133] BICEP, KECK collaboration, *Improved Constraints on Primordial Gravitational Waves using Planck, WMAP, and BICEP/Keck Observations through the 2018 Observing Season*, *Phys. Rev. Lett.* **127** (2021) 151301 [2110.00483].
- [134] A.R. Liddle and D.H. Lyth, *The Cold dark matter density perturbation*, *Phys. Rept.* **231** (1993) 1 [astro-ph/9303019].
- [135] R.H. Brandenberger, A. Nayeri, S.P. Patil and C. Vafa, *Tensor Modes from a Primordial Hagedorn Phase of String Cosmology*, *Phys. Rev. Lett.* **98** (2007) 231302 [hep-th/0604126].
- [136] M. Baldi, F. Finelli and S. Matarrese, *Inflation with violation of the null energy condition*, *Phys. Rev. D* **72** (2005) 083504 [astro-ph/0505552].
- [137] T. Kobayashi, M. Yamaguchi and J. Yokoyama, *G-inflation: Inflation driven by the Galileon field*, *Phys. Rev. Lett.* **105** (2010) 231302 [1008.0603].
- [138] G. Calcagni and S. Tsujikawa, *Observational constraints on patch inflation in noncommutative spacetime*, *Phys. Rev. D* **70** (2004) 103514 [astro-ph/0407543].
- [139] G. Calcagni, S. Kuroyanagi, J. Ohashi and S. Tsujikawa, *Strong Planck constraints on braneworld and non-commutative inflation*, *JCAP* **03** (2014) 052 [1310.5186].
- [140] J.L. Cook and L. Sorbo, *Particle production during inflation and gravitational waves detectable by ground-based interferometers*, *Phys. Rev. D* **85** (2012) 023534 [1109.0022].
- [141] S. Mukohyama, R. Namba, M. Peloso and G. Shiu, *Blue Tensor Spectrum from Particle Production during Inflation*, *JCAP* **08** (2014) 036 [1405.0346].
- [142] S. Kuroyanagi, T. Takahashi and S. Yokoyama, *Blue-tilted inflationary tensor spectrum and reheating in the light of NANOGrav results*, *JCAP* **01** (2021) 071 [2011.03323].
- [143] S. Kuroyanagi, T. Takahashi and S. Yokoyama, *Blue-tilted Tensor Spectrum and Thermal*

- History of the Universe, JCAP* **02** (2015) 003 [1407.4785].
- [144] LIGO SCIENTIFIC, VIRGO collaboration, *GW170104: Observation of a 50-Solar-Mass Binary Black Hole Coalescence at Redshift 0.2*, *Phys. Rev. Lett.* **118** (2017) 221101 [1706.01812].
- [145] LIGO SCIENTIFIC, VIRGO collaboration, *GW170608: Observation of a 19-solar-mass Binary Black Hole Coalescence*, *Astrophys. J. Lett.* **851** (2017) L35 [1711.05578].
- [146] LIGO SCIENTIFIC, VIRGO collaboration, *GW170814: A Three-Detector Observation of Gravitational Waves from a Binary Black Hole Coalescence*, *Phys. Rev. Lett.* **119** (2017) 141101 [1709.09660].
- [147] LIGO SCIENTIFIC, VIRGO collaboration, *GW170817: Observation of Gravitational Waves from a Binary Neutron Star Inspiral*, *Phys. Rev. Lett.* **119** (2017) 161101 [1710.05832].
- [148] LIGO SCIENTIFIC collaboration, *Advanced LIGO*, *Class. Quant. Grav.* **32** (2015) 074001 [1411.4547].
- [149] VIRGO collaboration, *Advanced Virgo: a second-generation interferometric gravitational wave detector*, *Class. Quant. Grav.* **32** (2015) 024001 [1408.3978].
- [150] LIGO SCIENTIFIC, VIRGO collaboration, *Open data from the first and second observing runs of Advanced LIGO and Advanced Virgo*, *SoftwareX* **13** (2021) 100658 [1912.11716].
- [151] L. Badurina, O. Buchmueller, J. Ellis, M. Lewicki, C. McCabe and V. Vaskonen, *Prospective sensitivities of atom interferometers to gravitational waves and ultralight dark matter*, *Phil. Trans. A. Math. Phys. Eng. Sci.* **380** (2021) 20210060 [2108.02468].
- [152] P.W. Graham, J.M. Hogan, M.A. Kasevich and S. Rajendran, *Resonant mode for gravitational wave detectors based on atom interferometry*, *Phys. Rev. D* **94** (2016) 104022 [1606.01860].
- [153] MAGIS collaboration, *Mid-band gravitational wave detection with precision atomic sensors*, 1711.02225.
- [154] L. Badurina et al., *AION: An Atom Interferometer Observatory and Network*, *JCAP* **05** (2020) 011 [1911.11755].
- [155] M. Punturo et al., *The Einstein Telescope: A third-generation gravitational wave observatory*, *Class. Quant. Grav.* **27** (2010) 194002.
- [156] S. Hild et al., *Sensitivity Studies for Third-Generation Gravitational Wave Observatories*, *Class. Quant. Grav.* **28** (2011) 094013 [1012.0908].

- [157] LIGO SCIENTIFIC collaboration, *Exploring the Sensitivity of Next Generation Gravitational Wave Detectors*, *Class. Quant. Grav.* **34** (2017) 044001 [1607.08697].
- [158] D. Reitze et al., *Cosmic Explorer: The U.S. Contribution to Gravitational-Wave Astronomy beyond LIGO*, *Bull. Am. Astron. Soc.* **51** (2019) 035 [1907.04833].
- [159] J. Baker et al., *The Laser Interferometer Space Antenna: Unveiling the Millihertz Gravitational Wave Sky*, 1907.06482.
- [160] J. Crowder and N.J. Cornish, *Beyond LISA: Exploring future gravitational wave missions*, *Phys. Rev. D* **72** (2005) 083005 [gr-qc/0506015].
- [161] V. Corbin and N.J. Cornish, *Detecting the cosmic gravitational wave background with the big bang observer*, *Class. Quant. Grav.* **23** (2006) 2435 [gr-qc/0512039].
- [162] C. Cutler and D.E. Holz, *Ultra-high precision cosmology from gravitational waves*, *Phys. Rev. D* **80** (2009) 104009 [0906.3752].
- [163] N. Seto, S. Kawamura and T. Nakamura, *Possibility of direct measurement of the acceleration of the universe using 0.1-Hz band laser interferometer gravitational wave antenna in space*, *Phys. Rev. Lett.* **87** (2001) 221103 [astro-ph/0108011].
- [164] K. Yagi and N. Seto, *Detector configuration of DECIGO/BBO and identification of cosmological neutron-star binaries*, *Phys. Rev. D* **83** (2011) 044011 [1101.3940].
- [165] AEDGE collaboration, *AEDGE: Atomic Experiment for Dark Matter and Gravity Exploration in Space*, *EPJ Quant. Technol.* **7** (2020) 6 [1908.00802].
- [166] A. Sesana et al., *Unveiling the gravitational universe at  $\mu$ -Hz frequencies*, *Exper. Astron.* **51** (2021) 1333 [1908.11391].
- [167] J. Garcia-Bellido, H. Murayama and G. White, *Exploring the early Universe with Gaia and Theia*, *JCAP* **12** (2021) 023 [2104.04778].
- [168] NANOGrAV collaboration, *The NANOGrav 11-year Data Set: Pulsar-timing Constraints On The Stochastic Gravitational-wave Background*, *Astrophys. J.* **859** (2018) 47 [1801.02617].
- [169] K. Aggarwal et al., *The NANOGrav 11-Year Data Set: Limits on Gravitational Waves from Individual Supermassive Black Hole Binaries*, *Astrophys. J.* **880** (2019) 2 [1812.11585].
- [170] NANOGrAV collaboration, *The NANOGrav 12.5 yr Data Set: Search for an Isotropic Stochastic Gravitational-wave Background*, *Astrophys. J. Lett.* **905** (2020) L34 [2009.04496].

- [171] T.J. Clarke, E.J. Copeland and A. Moss, *Constraints on primordial gravitational waves from the Cosmic Microwave Background*, *JCAP* **10** (2020) 002 [2004.11396].
- [172] M. Hazumi et al., *LiteBIRD: A Satellite for the Studies of B-Mode Polarization and Inflation from Cosmic Background Radiation Detection*, *J. Low Temp. Phys.* **194** (2019) 443.
- [173] A. Kogut, M.H. Abitbol, J. Chluba, J. Delabrouille, D. Fixsen, J.C. Hill et al., *CMB Spectral Distortions: Status and Prospects*, *Bull. Am. Astron. Soc.* **51** (2019) 113 [1907.13195].
- [174] J. Chluba et al., *Spectral Distortions of the CMB as a Probe of Inflation, Recombination, Structure Formation and Particle Physics: Astro2020 Science White Paper*, *Bull. Am. Astron. Soc.* **51** (2019) 184 [1903.04218].
- [175] X. Luo, W. Rodejohann and X.-J. Xu, *Dirac neutrinos and  $N_{eff}$ . Part II. The freeze-in case*, *JCAP* **03** (2021) 082 [2011.13059].
- [176] M. Maggiore, *Gravitational wave experiments and early universe cosmology*, *Phys. Rept.* **331** (2000) 283 [gr-qc/9909001].
- [177] R.H. Cyburt, B.D. Fields, K.A. Olive and T.-H. Yeh, *Big Bang Nucleosynthesis: 2015*, *Rev. Mod. Phys.* **88** (2016) 015004 [1505.01076].
- [178] CMB-HD collaboration, *Snowmass2021 CMB-HD White Paper*, 2203.05728.
- [179] CMB-BHARAT COLLABORATION collaboration, *Exploring Cosmic History and Origin: A proposal for a next generation space mission for near-ultimate measurements of the Cosmic Microwave Background (CMB) polarization and discovery of global CMB spectral distortions*, .
- [180] K.N. Abazajian and M. Kaplinghat, *Neutrino physics from the cosmic microwave background and large-scale structure*, *Annual Review of Nuclear and Particle Science* **66** (2016) 401 [<https://doi.org/10.1146/annurev-nucl-102014-021908>].
- [181] M. Alvarez et al., *PICO: Probe of Inflation and Cosmic Origins*, *Bull. Am. Astron. Soc.* **51** (2019) 194 [1908.07495].
- [182] CORE collaboration, *Exploring cosmic origins with CORE: Survey requirements and mission design*, *JCAP* **04** (2018) 014 [1706.04516].
- [183] SPT-3G collaboration, *SPT-3G: A Next-Generation Cosmic Microwave Background Polarization Experiment on the South Pole Telescope*, *Proc. SPIE Int. Soc. Opt. Eng.* **9153**

- (2014) 91531P [1407.2973].
- [184] SIMONS OBSERVATORY collaboration, *The Simons Observatory: Science goals and forecasts*, *JCAP* **02** (2019) 056 [1808.07445].
- [185] J.A. Casas, V. Di Clemente, A. Ibarra and M. Quiros, *Massive neutrinos and the Higgs mass window*, *Phys. Rev. D* **62** (2000) 053005 [hep-ph/9904295].
- [186] J. Elias-Miro, J.R. Espinosa, G.F. Giudice, G. Isidori, A. Riotto and A. Strumia, *Higgs mass implications on the stability of the electroweak vacuum*, *Phys. Lett. B* **709** (2012) 222 [1112.3022].
- [187] S. Vagnozzi, *Inflationary interpretation of the stochastic gravitational wave background signal detected by pulsar timing array experiments*, *JHEAp* **39** (2023) 81 [2306.16912].
- [188] S. Datta, *Explaining PTA Data with Inflationary GWs in a PBH-Dominated Universe*, 2309.14238.
- [189] J. Ellis, M. Fairbairn, G. Franciolini, G. Hütsi, A. Iovino, M. Lewicki et al., *What is the source of the PTA GW signal?*, *Phys. Rev. D* **109** (2024) 023522 [2308.08546].
- [190] J. Beacham et al., *Physics Beyond Colliders at CERN: Beyond the Standard Model Working Group Report*, *J. Phys. G* **47** (2020) 010501 [1901.09966].
- [191] A.M. Abdullahi et al., *The present and future status of heavy neutral leptons*, *J. Phys. G* **50** (2023) 020501 [2203.08039].
- [192] BABAR collaboration, *Experimental Searches For Heavy Neutral Leptons*, in *20th Conference on Flavor Physics and CP Violation*, 6, 2022 [2206.11422].
- [193] M.J. Dolinski, A.W.P. Poon and W. Rodejohann, *Neutrinoless Double-Beta Decay: Status and Prospects*, *Ann. Rev. Nucl. Part. Sci.* **69** (2019) 219 [1902.04097].
- [194] J.J. Gómez-Cadenas, J. Martín-Albo, J. Menéndez, M. Mezzetto, F. Monrabal and M. Sorel, *The search for neutrinoless double-beta decay*, *La Rivista del Nuovo Cimento* **46** (2023) 619.
- [195] G. Li, M.J. Ramsey-Musolf, S. Su and J.C. Vasquez, *Lepton number violation: From  $0\nu\beta\beta$  decay to long-lived particle searches*, *Phys. Rev. D* **105** (2022) 115018 [2109.08172].
- [196] Y. Cai, T. Han, T. Li and R. Ruiz, *Lepton Number Violation: Seesaw Models and Their Collider Tests*, *Front. in Phys.* **6** (2018) 40 [1711.02180].
- [197] D.J.H. Chung, E.W. Kolb and A. Riotto, *Production of massive particles during reheating*, *Phys. Rev. D* **60** (1999) 063504 [hep-ph/9809453].

- [198] F. Hahn-Woernle, M. Plumacher and Y.Y.Y. Wong, *Full Boltzmann equations for leptogenesis including scattering*, *JCAP* **08** (2009) 028 [0907.0205].
- [199] Y. Mambrini and K.A. Olive, *Gravitational Production of Dark Matter during Reheating*, *Phys. Rev. D* **103** (2021) 115009 [2102.06214].
- [200] M.A.G. Garcia, K. Kaneta, Y. Mambrini and K.A. Olive, *Reheating and Post-inflationary Production of Dark Matter*, *Phys. Rev. D* **101** (2020) 123507 [2004.08404].
- [201] A.D. Dolgov, *Introduction to Cosmology*, *Phys. Atom. Nucl.* **73** (2010) 815 [0907.0668].